Hiding in the yolk: a unique feature of *Legionella pneumophila* infection of zebrafish

Flávia Viana[1,§], Laurent Boucontet[2,§], Valerio Laghi[2], Daniel Schator[1,3], Marine Ibranosyan[4], Sophie Jarraud[4,5], Emma Colucci-Guyon[2§*] and Carmen Buchrieser[1§*]

[1]Institut Pasteur, Université Paris Cité, Biologie des Bactéries Intracellulaires and CNRS UMR 6047 75724, Paris, France, [2]Institut Pasteur, CNRS UMR 3738, Paris, France, [3]Sorbonne Université, Collège doctoral, 75005 Paris, France, [4]National Reference Centre of *Legionella*, Institute of Infectious Agents, Hospices Civils de Lyon, Lyon, France, [4] Hospices Civils de Lyon, Centre National de Référence des Legionella, Lyon, France, [5]Centre International de Recherche en Infectiologie, Université Lyon 1, UMR CNRS 5308, Inserm U1111, ENS de Lyon, Lyon, France

§ These authors contributed equally

Key words: *Legionella pneumophila*, zebrafish, yolk sac, innate immune response; live imaging; neutrophils; macrophages

[*]For correspondence:

Carmen Buchrieser
Institut Pasteur
Biologie des Bactéries Intracellulaires
28, rue du Dr. Roux, 75724
Paris Cedex 15
France
E-mail: *cbuch@pasteur.fr*

Emma Colucci-Guyon
Institut Pasteur
CNRS UMR 3738
25, rue du Dr. Roux, 75724
Paris Cedex 15
France
E-mail: *emma.colucci@pasteur.fr*

Abstract

The zebrafish has become a powerful model organism to study host-pathogen interactions. Here, we developed a zebrafish model of *Legionella pneumophila* infection to dissect innate immune responses. We show that *L. pneumophila* cause zebrafish larvae death in a dose dependent manner, and that macrophages are the first line of defence, with neutrophils cooperating to clear the infection. When either macrophages or neutrophils are depleted, these "immunocompromised" larvae become lethally sensitive to *L. pneumophila* similar to what is known for humans that develop pneumonia. Also as observed in human infections, the adaptor signalling molecule Myd88 is not required to control disease in the larvae. Furthermore, proinflammatory cytokine genes *il1β* and *tnfα* were upregulated during infection, recapitulating key immune responses seen in human infection. Strikingly, we uncovered a previously undescribed infection phenotype in zebrafish larvae, whereby bloodborne, wild type *L. pneumophila* invade and grow in the larval yolk region, a phenotype not observed with a type IV secretion system deficient mutant that cannot translocate effectors into its host cell. Thus, zebrafish larva represents an innovative *L. pneumophila* infection model that that on one hand mimics important aspects of the human immune response to *L. pneumophila* infection and that on the other hand will allow to elucidate the mechanisms by which type IV secretion effectors allow *L. pneumophila* to cross membranes and to obtain nutrients from nutrient rich environments.

INTRODUCTION

Legionella pneumophila, a gram negative, facultative intracellular bacterium inhabits natural, freshwater sources [1, 2]. As an environmental, aquatic microbe *L. pneumophila* replicates intracellularly in aquatic protozoa [3]. Most interestingly, in contrast to other intracellular pathogens *L. pneumophila* is not adapted to a single host, but it exhibits a broad host range including Amoebozoa (amoebae), Percolozoa (excavates) and Ciliophora (ciliated protozoa) [3, 4]. In the environment *L. pneumophila* can also be found within biofilms where it acquires nutrients from this mixed community, but it can also survive in a planktonic form for a certain time [5]. As fresh water and man-made systems are connected, *L. pneumophila* can also contaminate artificial water systems. Protected within its protozoan hosts *L. pneumophila* survives water disinfectants and may infect humans *via* aerosols produced by different man-made structures and devices. The inhalation of *L. pneumophila*-contaminated aerosols can cause a severe pneumonia, the so-called Legionnaires' disease [6]. However, not every infection leads to disease. Disease outcome is determined by virulence of the bacterial strain, the bacterial burden in the inhaled aerosols and most importantly by the host immune status. Host factors determining susceptibility include age above 50, smoking and/or having chronic lung disease, being immunocompromised and genetic factors that alter the immune response [2, 7, 8].

Once the bacteria reach the lungs of susceptible individuals, they can infect alveolar macrophages and replicate therein. After being phagocytosed *L. pneumophila* avoids lysosomes and establishes an endoplasmic reticulum derived vacuole named the *Legionella* containing vacuole (LCV) [9, 10]. The LCV, a safe haven for bacterial replication, is established by utilizing the Dot/Icm type IV secretion system (T4SS) that injects over 330 proteins into the host cell [9-11]. These effector proteins manipulate a myriad of host pathways to recruit vesicles derived from the endoplasmic reticulum to the LCV, to supply the bacteria with nutrients, restrain autophagy and supress apoptosis and to subvert the host cell immune response [9-11]. A surprising high number of these effectors mimic host proteins and encode eukaryotic functions helping *L. pneumophila* to modulate numerous host pathways to its own benefit in remarkable diverse ways [11-13]

Intracellular replication of *L. pneumophila* and innate immune responses to this pathogen have been studied *in vitro* using both murine and human cell lines and *in vivo* using different animal models of infection. However, results obtained with these models cannot be easily extrapolated to what is observed in human disease. Studies in invertebrate models, such as *Galleria mellonella* and *Caenorhabditis elegans*, [14, 15] require further validation in more developed models as their immune system greatly differs from that of vertebrates. Interestingly, mouse infection fails to recall the human disease phenotype, as most inbred mice strains are naturally resistant to *L. pneumophila* [16]. Very early after the discovery of *L. pneumophila* the guinea pig model of Legionnaires' disease

95 was developed as these are highly susceptible to *L. pneumophila* when infected through injection
96 into the peritoneum [6] or when exposed to *L. pneumophila* containing aerosols [6]. Several studies
97 thereafter have shown that the guinea pig infection model recalls human disease and allows to study
98 the immune response to *L. pneumophila* infection [17, 18]. However, the guinea pig model is rarely
99 used due to the limited availability of specific immunological reagents for these animals and the
100 demanding laboratory and husbandry requirements.

101 The above-mentioned models, including the widely used murine models, present limitations
102 for studying *L. pneumophila* infection *in vivo* and discrepancies exist between results obtained in
103 mouse or human cells, as for example mouse macrophages restrict *L. pneumophila* growth via
104 caspase 1 and caspase 7 activation whereas human macrophages do not activate caspase 1 and 7
105 and thus allow growth of *L. pneumophila* [19, 20]. Thus, we sought to develop a new, alternative
106 model for *Legionella* infection. The zebrafish (*Danio rerio*) originally introduced as a model organism
107 in developmental biology has emerged in recent years as a powerful non-mammalian model to study
108 nearly every aspect of biology, including immune cell behaviour and host-pathogen interactions [21,
109 22]. Zebrafish are evolutionary closer to humans than fruit flies and nematodes, easier to manipulate
110 than mice and their immune system is remarkably similar to the one of mammals, making them an
111 attractive laboratory model for immunology and infection biology [21, 22]. Its popularity is also due
112 to its small size and the natural translucency of its embryos and larvae, which makes it possible to
113 follow leukocyte behaviour and infection onset at the level of the whole organism in real-time and
114 high resolution [23]. Additionally, although adult organisms display a fully developed immune system
115 with both active innate and adaptive branches, studies can also be conducted at the early stages of
116 life (embryonic or larvae) when the organism solely relies on innate immunity, allowing to dissect the
117 mechanisms arising from different immune responses [23-25]. Here we examined whether the
118 zebrafish could be an alternative model for analysing host-pathogen interactions and the innate
119 immune response to *L. pneumophila* infection.

120 We show that *L. pneumophila* infection of zebrafish larvae recapitulate human disease onset,
121 as infected wild-type larvae are generally able to clear the infection, but immunocompromised fish
122 fail to do so. Both macrophages and neutrophils quickly interact and engulf injected *L. pneumophila*.
123 Macrophage-depleted larvae show a dramatic increase of bacterial burden concomitant with host
124 death, pointing to a crucial role of macrophages in controlling the infection. However, not all larvae
125 are able to control the infection, but a fraction showed high bacterial burden in the yolk region, a
126 unique zebrafish infection phenotype.

127

128 **RESULTS**

129 ***L. pneumophila infection induces mortality in zebrafish larvae in a dose dependent manner***

130 To analyse whether *L. pneumophila* can cause disease in zebrafish larvae we microinjected larvae 72
131 hours post fertilisation (hpf) intravenously in the caudal vessels near the cloaca (Fig 1A), with 10^3 or
132 10^4 CFU of wild type (WT) *L. pneumophila* strain Paris expressing GFP (WT-GFP) or the type IV
133 secretion system (T4SS) deficient isogenic mutant expressing GFP (Δ*dotA*-GFP). The infected larvae
134 were kept at 28°C and were monitored regularly until 72 hours post infection (hpi) to record survival
135 or death using a stereomicroscope. Larvae infected with doses of up to $2x10^3$ CFU of WT-GFP
136 (defined as low dose, LD) all survived (100% survival). In contrast, larvae infected intravenously with
137 doses of 10^4 CFU (defined as high dose, HD) resulted in approximately 30% of death within 72 hpi (Fig
138 1B). Importantly, all larvae injected with HD of the Δ*dotA*-GFP strain survived for the entire time of
139 observation (Fig 1B) indicating that the T4SS is crucial for replication in zebrafish larvae as it is in
140 other infection models and in humans.

141 We then set up a method to monitor the bacterial burden of the infected zebrafish larvae.
142 The progression of the infection was followed by analysing the bacterial load at 0, 24, 48 and 72 hpi
143 comparing three different methods. First, we quantified the pixel counts of GFP fluorescence of live
144 larvae images (Fig. S1A), secondly, we analysed the number of GFP expressing bacteria present in
145 lysed infected larvae by FACS (Fig. S1B) and thirdly we plated serial dilutions of homogenates of
146 euthanized larvae on BCYE medium (Fig S1C). The results obtained with the three methods showed a
147 similar trend, but the method using fluorescent pixel counts on live injected larvae seemed to most
148 accurately represent the bacterial load. Thus, we choose to monitor the *L. pneumophila* load of
149 zebrafish larvae by fluorescent pixel counts on live injected larvae, and in addition by FACS on lysed
150 larvae at various time points, using the GFP fluorescence of the bacteria. As shown in Fig. 1C, where
151 the bacterial burden was evaluated by fluorescent pixel counts on individual injected larvae followed
152 over 72hpi, most larvae injected with LD of WT-GFP progressively control the bacteria by 24 hpi with
153 only few larvae showing an increase in bacterial numbers at 72hpi. Similarly, HD of Δ*dotA*-GFP were
154 also progressively controlled by 24 hpi. In contrast, some zebrafish larvae injected with HD of WT-
155 GFP were unable to eliminate the bacteria at 72hpi, and the bacterial counts remained high and
156 increased by 48-72 hpi (Fig 1C). These results were corroborated by FACS analysis on lysed larvae (Fig
157 S2 A). We also monitored infected larvae by fluorescence microscopy. Immediately upon injection
158 (20 min to 2 hpi), bacteria were detectable as small foci, probably associated with professional
159 phagocytes (Fig. 1D). By 24 hpi, in both, larvae injected with LD of WT-GFP as well as larvae injected
160 with HD of the avirulent Δ*dotA*-GFP strain, the GFP signal declined becoming undetectable by 48 hpi,
161 suggesting that the bacteria were progressively cleared. Despite showing the same pattern at 24 hpi,
162 larvae injected with HD of WT-GFP showed an increase in GFP signal at 48 hpi, suggesting that
163 bacterial proliferation occurred in a fraction of the infected larvae. Interestingly, in these larvae,

164 bacterial proliferation occurred mainly in the yolk region where the bacterial foci increased
165 dramatically over time, with concomitant death of the infected larvae by 72 hpi (Fig 1D).
166 To gain insight into the progression of the infection, we analysed the bacterial presence in
167 the yolk or in the rest of the body (tail + trunk + head) of LD and HD WT-GFP or HD Δ*dotA*-GFP
168 infected larvae under the fluorescence microscope over time. A single small GFP dot (indicating few
169 bacteria) present in the larvae was scored as "positive for infection". We observed that about 60% of
170 larvae injected with HD WT-GFP and about 20% of larvae injected with LD WT-GFP showed yolk
171 growth at 72 hpi. In contrast, larvae injected with HD Δ*dotA*-GFP progressively cleared the bacteria,
172 and bacteria were never observed growing in the yolk (Fig 1E, F; Figure 3D). The presence of bacteria
173 in the yolk was intriguing and prompted us to investigate whether this unique feature was
174 dependent on the site of injection of bacteria in the larvae. Thus, we injected 72hpf zebrafish larvae
175 with HD WT-GFP in different closed cavities such as the otic vesicle and the hind brain ventricle. The
176 survival, bacterial burden, and outcome of bacterial dissemination over time compared to
177 bloodstream injected bacteria showed that only blood borne bacteria can successfully replicate in
178 zebrafish and establish a proliferative niche in the yolk. This suggests a role of the blood circulation in
179 the capacity of *L. pneumophila* to reach the yolk region and to replicate there (Fig S3 A-C).
180 Secondly, we tested if a natural route of uptake could cause infection in zebrafish. As in its
181 usual habitat *L. pneumophila* lives in freshwater and replicates in protozoan hosts [26] it is possible
182 that fish get infected in the environment by taking up infected amoeba. Indeed, amoebae are prey of
183 zebrafish larvae. To test this hypothesis, we infected *A. castellanii* with *L pneumophila* and exposed
184 120hpf zebrafish larvae (start of autonomous feeding) to *L. pneumophila* infected amoebae and
185 evaluated bacterial survival (Fig S4 A) and bacterial dissemination (Fig S4 B-D) in the larvae over time.
186 While zebrafish larvae engulfed the infected amoebae, as shown by the GFP signal detectable in the
187 exposed larvae at 48 hours post contact bath (Fig S4C), no permanent infection was established and
188 the engulfed bacteria were evacuated with other faecal content without impact on larvae survival,
189 suggesting that this might not be an important route of infection in the environment.
190 Collectively these results indicate that only bloodstream injected WT *L. pneumophila* induce
191 a dose dependent death of zebrafish larvae. Larvae that were unable to control infection by 48 hpi,
192 showed a unique infection phenotype, a high increase of the bacterial burden in the yolk region.
193
194 ***Legionella pneumophila replication in the yolk of zebrafish larvae is T4SS dependent***
195 The replication of *L. pneumophila* in the yolk region of infected zebrafish larvae was strictly
196 dependent on a functioning T4SS as Δ*dotA*-GFP failed to reach the yolk. To investigate whether the
197 secretion mutant can grow in the yolk cell when reaching it, we injected LD and HD of WT-GFP or of
198 Δ*dotA*-GFP *L. pneumophila* directly into the yolk cell cytoplasm of 72hpf zebrafish larvae (Fig. 2A).

199 Surprisingly, Δ*dotA*-GFP did not replicate in the yolk even when injected directly although it persisted
200 over 48hpi (Fig 2B, C, Fig S2B). WT-GFP replicated in the yolk region both, upon LD and HD injections
201 resulting in an increased bacterial proliferation in the yolk and subsequent death of the larvae
202 whereby 100% of the larvae dying have bacteria replicating in the yolk. (Fig 2B, C, Fig S2B). These
203 observations suggest that T4SS system is not only crucial for reaching the yolk region but likely that
204 some of its effectors are necessary for the bacteria to obtain nutrients from the yolk environment to
205 allow replication. To further analyse this hypothesis, we selected a mutant in the gene encoding a
206 sphingosine-1 phosphate lyase, (WT, Δ*spl)* [27] as we reasoned that this enzyme might be implicated
207 in degrading sphingolipids present in the yolk of zebrafish larvae and thereby might aid
208 *L. pneumophila* to obtain nutrients. Injection of Δ*spl* in the yolk sac region*,* and analyses of larvae
209 death as compared to WT or Δ*dotA* showed that survival of zebrafish larvae injected with the Δ*spl*
210 was slightly but significantly higher than with WT injected larvae (Fig. S5A)*,* suggesting that the T4SS
211 effector *Lp*Spl might be implicated in nutrient acquisition in the yolk environment.
212 Interestingly, the first isolation of *L. pneumophila* was achieved by inoculating the yolk region
213 of embryonated eggs probably due to the richness in nutrients provided by the yolk [6]. Thus, we
214 decided to investigate the infection phenotype of *L. pneumophila* WT and Δ*dotA* in the yolk sac
215 further using as model embryonated chicken eggs (ECE). We inoculated ECE directly in the yolk
216 region with WT and with the Δ*dotA* strain at a concentration of 9.2 $\log_{10}$ CFU/mL and 9.1 $\log_{10}$
217 CFU/mL, respectively and assessed mortality of the embryos daily. The survival curves were
218 significantly different (p=0.0111). The total mortality during the 6-day observation period was
219 significantly higher in WT-GFP infected eggs (88.9%) than in the Δ*dotA*-infected eggs (14.3%) or PBS
220 inoculated control eggs (28.6%) (Fig. S5C). The highest mortality was observed at 2 days post
221 infection in WT inoculated eggs with 55.6% mortality *versus* 0% in Δ*dotA* or 28.6% mortality in PBS
222 inoculated eggs. Quantification of *L. pneumophila* in the yolk sac region at the day of mortality or at
223 day 6 post infection revealed that the number of bacteria in the yolk sac of WT-infected ECE, was
224 significantly higher than that in the yolk sac of those infected with the Δ*dotA* strain (7.8 $\log_{10}$ CFU/mL
225 and 5.9 $\log_{10}$ CFU/mL, respectively, p=0.0127) (Fig. S5D). Controls inoculated with PBS (n=2) showed
226 no *L. pneumophila* growth. Thus, like in zebrafish larvae only the WT strain can replicate in the yolk
227 region and of inducing mortality in the embryos, while the T4SS mutant strain persists but is not able
228 to replicate and does not induce high embryo mortality. This result further supports the finding that
229 the T4SS system is crucial for obtaining nutrients when lipids are the major available energy source.
230 Taken together, these results suggest that the *L. pneumophila* T4SS plays a crucial role for
231 the bacteria to pass from the blood circulation into the yolk and that T4SS effectors play an
232 important role to obtain nutrients for bacterial proliferation in the yolk.

233 ***Bloodstream L. pneumophila establishes a proliferative niche in the yolk region causing a persistent***
234 ***infection***
235 To characterise the *L. pneumophila* foci identified in the yolk region of zebrafish larvae, we used high
236 resolution fluorescence microscopy of HD of WT-GFP *L. pneumophila* injected in the bloodstream of
237 72hpf zebrafish larvae and analysed them at 72hpi. This analysis confirmed that these bacterial
238 structures localize in the yolk and or in the yolk tube region (Fig. 2D, Movie S1). *L. pneumophila* foci
239 in the yolk region are highly complex, aggregate-like structures of long, filamentous bacteria.
240 Moreover, upon injection of HD WT-GFP in Tg(*kdrl*::mCherry)^{is5} (red blood vessels) larvae, we showed
241 that the fast growing bacterial aggregates localize close to the blood vessels, mostly below and
242 probably above the yolk cell. Single bacteria near the aggregates localized within the blood vessels,
243 indicating that the bacteria can cross the endothelial barrier to reach the yolk region (Fig 2E, Movie
244 S2). To analyse macrophage and neutrophil interactions with the bacterial aggregates in the yolk
245 region, we injected HD WT-GFP in Tg*(mfap4::mCherryF*) (herein referred as *mfap4*:mCherryF) (red
246 macrophages) or Tg(*Lyz::DsRed)*^{nz50} (herein referred as *lyz*:DsRed)(red neutrophils) or
247 Tg(*kdrl*::mCherry)^{is5} (red blood vessels) zebrafish larvae. At 72hpi macrophages accumulated around
248 the yolk region containing *L. pneumophila* but did not seem to be able to engulf the bacterial
249 aggregates. (Fig. 3A, Movie S3). Similarly, upon injection of HD of WT-GFP in *lyz*:DsRed larvae (red
250 neutrophils), at 72hpi neutrophils accumulated around the growing bacterial aggregates, but seemed
251 also unable to engulf them (Fig 3B, C, Movie S4). Strikingly, quantification analyses showed that
252 bacterial colonisation of the yolk of zebrafish larvae injected with the T4SS deficient Δ*dotA* mutant
253 strain, did never take place, suggesting that zebrafish susceptibility to *L. pneumophila* infection and
254 yolk penetration depends on a functional T4SS system (Fig. 3D). It should be noted that the yolk is
255 the only food source of the larvae during this developmental stage. The fast proliferation of the
256 bacteria in the yolk region probably depletes its nutritional content, leading to larvae death.
257 To gain deeper insight into the exact anatomical localisation of the bacteria in the yolk
258 region, we performed high resolution confocal time lapse acquisitions of HD of WT-GFP bloodstream
259 injected larvae harbouring red macrophages between 48 and 72hpi. We observed that
260 *L. pneumophila* foci seem to localize both above but also below the plasmatic yolk membrane,
261 suggesting that they can cross it, and that professional phagocytes remain above the growing
262 bacterial aggregates failing to engulf them (Fig 3E, Movie S5). Live imaging showed that both
263 macrophages and neutrophils accumulated around bacteria proliferating in the yolk region. To
264 investigate if professional phagocytes were recruited to the bacteria from other sites, or if only the
265 population located on the yolk was involved, we quantified macrophages and neutrophils in the body
266 and in the yolk of the whole larva overtime, focusing on HD WT-GFP infected larvae. We then
267 separated the larvae with bacterial burden in the yolk from the total population of infected larvae, to

268 specifically analyse the recruitment of professional leukocytes to the bacteria growing in the yolk.
269 Following the same criteria as above, we quantified the bacterial burden of the infected larvae over
270 time. This quantitative analysis showed that macrophages and neutrophils that accumulated where
271 the bacteria are seen in the yolk by 48hpi, were the ones located on the yolk surface, and that no
272 professional phagocyte population was recruited in the other parts of the body (Fig 3F; Fig S6).
273 Moreover, this analysis confirmed that the bacterial burden increased in the yolk while decreasing in
274 the body (Fig 1E) and it also revealed a decrease of professional phagocyte populations in infected
275 larvae upon HD WT-GFP injection overtime.
276 Thus, blood-borne *L. pneumophila* can invade the yolk sac of zebrafish larvae, a previously
277 undescribed phenotype of bacterial infection in this model. Once in the yolk, the bacteria replicate
278 extensively, forming complex, organized, aggregate-like structures that cannot be removed by
279 macrophages and neutrophils, thereby avoiding the host's immune control and clearance, and
280 eventually causing the death of the larvae.
281
282 ***Infection of zebrafish larvae with high doses of L. pneumophila leads to macrophage and***
283 ***neutrophil death***
284 In human infection, alveolar macrophages are the primary cell type infected by *L. pneumophila*
285 supporting its intracellular replication. Following infection, neutrophils are recruited to the lung and
286 are key players for controlling infection as they possess antimicrobial activity and kill *L. pneumophila*
287 [28]. Moreover, the analysis of the recruitment of professional leukocytes to the bacteria in the yolk
288 of HD WT-GFP infected larvae revealed a decrease of professional phagocyte populations overtime
289 (Fig 3F). Thus, to analyse whether zebrafish infection mirrors human infection, we monitored the
290 behaviour of zebrafish macrophages or neutrophils over time. The transgenic zebrafish larvae
291 *mfap4*:mCherryF and *lyz*:DsRed were injected with low or high doses of WT-GFP or with high doses of
292 Δ*dotA*-GFP. Infected live larvae were monitored using widefield fluorescence microscopy and the
293 number of leukocytes per larva was assessed by counting fluorescent macrophages and neutrophils
294 over time until 72hpi. We observed that upon injection of high dose WT-GFP, the macrophage count
295 decreased dramatically at 24hpi and 48hpi, but started to increase at 72hpi (Fig. 4A). Neutrophil
296 counts gave similar results at 24 and 48hpi upon injection of high doses of WT bacteria, as there was
297 a dramatic decrease observed in neutrophil numbers by 24hpi. However, the neutrophil counts were
298 still decreased at 72hpi (Fig. 5A). In contrast macrophage and neutrophil counts remained unaffected
299 upon injection of equal amounts of the avirulent Δ*dotA* strain, with a slight increase of neutrophil
300 numbers at 72hpi, suggesting that phagocyte death is linked to a functional T4SS system (Fig 4A, 5A).
301

302 Taken together, these results show that high dose *L. pneumophila* infection leads to a
303 decrease in the number of professional phagocytes dependent on the T4SS, like what is seen during
304 human infection by *L. pneumophila* or *Mycobacterium tuberculosis* [28, 29]
305
306 ***Macrophages are the primary cells to phagocytise blood-borne L. pneumophila and neutrophils co-***
307 ***operate to decrease bacterial load***
308 As macrophages and neutrophils are the phagocytes known to firstly interact with *L. pneumophila* we
309 analysed phagocyte-*L. pneumophila* interactions *in vivo* by injecting *mfap4*:mCherryF or *lyz*:DsRed
310 72hpf larvae with WT-GFP or Δ*dotA*-GFP and recorded phagocyte-*L. pneumophila* interactions using
311 high resolution confocal microscopy. This showed that upon injection of LD WT-GFP, macrophages
312 immediately contacted and engulfed blood-borne bacteria. Macrophages were continuously
313 recruited to the site of injection and by 16hpi the bacteria were mostly undetectable while
314 macrophage numbers increased (Fig. 4B top panel, Movie S6). Macrophages that had engulfed a
315 large amount of *L. pneumophila* stopped moving and rounded-up. Similarly, the inhibition of the
316 migration of phagocytes by *L. pneumophila* has been observed previously during infection of RAW
317 264.7 macrophages and the amoeba *Dictyostelium discoideum* and *Acanthamoeba castellanii*, [30,
318 31]. In contrast, zebrafish injected with HD of WT-GFP were not able to restrict the bacterial growth
319 by 16hpi. Injection of HD of *L pneumophila* led to the formation of big bacterial aggregates, that were
320 not easily engulfed and cleared by macrophages, as previously shown for bacterial aggregates
321 proliferating in the yolk region (Fig 4B, second panel, Movie S6). Remarkably, macrophages were very
322 efficient in engulfing and rapidly clearing high doses and big bacterial aggregates of blood-borne
323 Δ*dotA*-GFP bacteria. By 10hpi most of the Δ*dotA* bacteria and bacterial aggregates had been engulfed
324 and cleared as suggested by the diffuse GFP staining in phagocytes (Fig. 4B, bottom panel, Movie S6).
325 However, upon infection with a HD WT-GFP, bacteria were not completely cleared and at 72hpi live
326 *L. pneumophila* were found in macrophages, suggesting that the bacteria are also replicating in
327 macrophages of zebrafish larvae. Indeed, high resolution confocal microscopy showed that at 72hpi,
328 *L. pneumophila* can also be found inside of macrophages in structures resembling replicative
329 vacuoles (Fig. 4C).
330 The analyses of *L. pneumophila*-neutrophil interactions showed that these cells engulfed the
331 bacteria trapped in the mesenchyme around the site of injection, but they were less efficient at
332 clearing blood-borne bacteria. This has also been previously observed for infection of zebrafish
333 larvae with *Escherichia coli* or *Shigella flexneri* [24, 32]. Indeed, upon injection with a HD of WT-GFP,
334 neutrophil failed to restrict *L. pneumophila*, leading to massive death of infected neutrophils, they
335 rounded up and lost their fluorescence (Fig. 5B, second panel; Movies S7; Fig 5C; Movie S8). In sharp
336 contrast, neutrophils very efficiently engulfed and cleared large amounts of Δ*dotA*-GFP aggregated

337 and trapped in the mesenchyme (Fig. 5B, lower panel, Movie S7) as well as low doses of WT-GFP (Fig
338 5B upper panel, Movie S7).
339 Altogether this shows that upon low dose bloodstream injection of *L. pneumophila*,
340 macrophages and neutrophils efficiently cooperate to eliminate most of the injected bacteria within
341 20-24 hpi, with macrophages playing the primary role. However, *L. pneumophila* seems to persist
342 upon high dose WT-GFP injection, and the observation of structures resembling large vacuoles
343 containing live *L pneumophila* at 72hpi suggests that they can replicate in zebrafish macrophages. In
344 contrast, neutrophils interact with *L. pneumophila* by quickly engulfing bacteria trapped in the
345 mesenchyme near the site of injection but are less efficient in clearing blood-borne bacteria.
346
347 ***Macrophages are the first line defence restricting L. pneumophila infection***
348 In humans, innate immune responses, based essentially on the activity of professional phagocytes
349 and the induction of pro-inflammatory cytokine genes, are the key players to control and restrict
350 *L. pneumophila* proliferation. Hence, human disease develops primarily in immunocompromised
351 individuals [10]. To investigate whether the phagocytes of the innate immune system, macrophages
352 and neutrophils, are also responsible for controlling *L. pneumophila* infection in zebrafish larvae, we
353 selectively and transiently depleted macrophages or neutrophils, and infected these
354 "immunocompromised" larvae with *L. pneumophila*. Depletion of macrophages was achieved by
355 knocking down the expression of s*pi1b*, a transcription factor involved in early myeloid progenitor
356 formation. A low dose of s*pi1b* morpholino was reported to impact macrophages without affecting
357 neutrophils [33]. We monitored the effect of low doses s*pi1b* morpholino injection on macrophage
358 and neutrophil populations in double transgenic larvae with green neutrophils (*mpx*:GFP) and red
359 macrophages (*mfap4*:mCherryF). The specific depletion of macrophages was confirmed by counting
360 macrophages and neutrophils at 72hpf (Fig S7A).
361 We then infected macrophage depleted larvae (s*pi1b* knockdown) by intravenous injection of
362 LD or HD of WT-GFP. Regardless of the infection dose, a dramatic decrease in larvae survival was
363 observed, as even injection of low doses of WT-GFP resulted in the death of 30% of the larvae (Fig
364 6A). When injecting high doses of WT-GFP nearly all the infected larvae died by 72hpi, with the
365 earliest deaths starting 48hpi (Fig 6A). In contrast, s*pi1b* knockdown larvae injected with high doses
366 of Δ*dotA*-GFP did not show impaired survival (Fig 6A). The increased mortality correlated with an
367 increased but not significantly different bacterial burden in the s*pi1b* knockdown larvae compared to
368 control larvae (Fig 6B, Fig S2C). Intravital imaging of infected s*pi1b* knock down larvae also showed
369 that both low and high doses of WT-GFP failed to be cleared and that the bacteria established a
370 replicative niche in the yolk, where they proliferated extensively (Fig 6C). This highlights, that
371 macrophages are critical to restrict the onset of infection and *L. pneumophila* proliferation *in vivo*.

372 Furthermore, these results also suggest that neutrophils, which are not depleted in s*pi1b* knockdown
373 larvae, fail to control *L. pneumophila* infection in the absence of macrophages.
374 To analyse the role of neutrophils in controlling the infection, neutrophil development was
375 disrupted by knocking down the G-CSF/GCSFR pathway using *csf3R* morpholino, previously reported
376 to decrease up to 70% of the neutrophils present [34-36]. We monitored the efficiency of the *csf3R*
377 morpholino knockdown in double transgenic larvae confirming that 75% of the neutrophil population
378 was depleted, while macrophage numbers were only slightly decreased (Fig S7B). When HD Δ*dotA*-
379 GFP was injected, neutrophil-depleted larvae survived, and the bacterial burden remained
380 unchanged, like what we had observed in infections of macrophage-depleted larvae (Fig. 6D, E).
381 However, when neutrophil-depleted larvae were injected with HD WT-GFP, larvae survival
382 significantly decreased and bacterial burdens slightly increased by 48hpi (Fig. 6D, E; FigS2D).
383 Intravital imaging showed that *csf3R* knockdown larvae that were unable to control *L. pneumophila*
384 infection showed bacterial proliferation in the yolk comparable to WT control larvae (Fig 6F).
385 These results show that both macrophages and neutrophils are required for restricting and
386 controlling *L. pneumophila* infection in the zebrafish model, but macrophages play the main role.
387 Although neutrophils contributed less to clear the bacteria upon bloodstream injection, neutrophils
388 might impact the infection outcome through cytokine release that can modulate macrophage
389 activity.
390
391 ***Key pro-inflammatory cytokine genes are induced upon L. pneumophila infection of zebrafish***
392 ***larvae***
393 Proinflammatory cytokines produced by infected and bystander cells during *L. pneumophila* infection
394 of humans and mice play crucial roles in orchestrating host defences to control infection [37, 38].
395 Infected cells produce IL-1α and IL-1β through a mechanism involving MyD88-dependent
396 translational bypass. In contrast, bystander cells produce IL-6, TNF-α and IL-12 in an IL-1 receptor (IL-
397 1R) dependant way [37, 39]. To determine the pro-inflammatory responses of zebrafish larvae during
398 *L. pneumophila* infection, we analysed *il1b*, *tnfa*, and *ifng1/2* (orthologues of mammalian *Ifng*) gene
399 expression levels over time by qRT-PCR on RNA isolated from individual infected larvae. We found
400 that infection of zebrafish larvae with LD or HD of WT-GFP induced a rapid (by 6hpi) and robust
401 induction of *il1b* and *tnfa* gene expression. In larvae injected with low doses of WT-GFP the
402 expression levels started to decrease by 24hpi, and gradually became undetectable at 72hpi. In
403 contrast, larvae injected with HD of WT-GFP, expression of *il1b* and *tnfa* did not decrease over time
404 (Fig. 7A and B) and a significant induction of *ifng1* was observed at 48hpi (Fig. 7C) but not of *ifng2*
405 (Fig. 7D). In parallel, we scored the bacterial burden of the infected larvae before the measurement
406 of pro-inflammatory cytokine gene induction at each time point under the microscope, which

407 consistently showed that larvae with increased *il1b* and *tnfa* induction had also high bacterial
408 burdens in the yolk and were not controlling the infection (Fig S8A). These pro-inflammatory
409 responses were T4SS dependent, as zebrafish larvae infected with HD of Δ*dotA*-GFP did not show
410 significant induction of transcription of *tnfa*, *il1b* and *ing1/2* (Fig. 7 A-D).
411 Collectively, these results reveal, that key pro-inflammatory cytokines known to orchestrate
412 the host response during *L. pneumophila* infection in humans are also induced in zebrafish larvae,
413 and that cytokine gene induction is sustained when uncontrolled *L. pneumophila* proliferation occurs.
414
415 ***The immune response of zebrafish larvae to L. pneumophila infection is independent of MyD88***
416 ***signalling***
417 In innate immunity, the myeloid differentiation factor 88 (MyD88) plays a pivotal role in immune cell
418 activation through Toll-like receptors (TLRs). MyD88-deficient mice are highly susceptible to
419 *L. pneumophila* infection [40-43], however this is not the case when human macrophages are
420 depleted of MyD88 [44]. Therefore, we sought to analyse which role MyD88 plays in zebrafish larvae
421 during *L. pneumophila* infection. We injected *myd88-/-* and control larvae with LD or HD of WT-GFP,
422 or with HD of Δ*dotA*-GFP and monitored larvae survival and bacterial burden over time as described
423 in Figure 1. Our results show that susceptibility to infection of *myd88-/-* larvae injected with HD of
424 WT-GFP was comparable to that of WT larvae, as only a very slight, but no significant increase of the
425 bacterial burden was observed in *myd88-/-* larvae by 24hpi. *L. pneumophila* Δ*dotA*-GFP did not
426 establish an infection, and the bacterial burden decreased over time indicating that bacteria were
427 cleared (Fig. 7E, F; Fig S2E). To determine if pro-inflammatory responses were affected in the
428 absence of MyD88 signalling, we analysed *il1b*, *tnfa* and *ing1/2* gene expression levels over time in
429 control and *myd88-/-* larvae. Our results showed that *il1b, tnfa* and *ing1/2* gene expression levels
430 were comparable in control and *myd88-/-* infected larvae for all tested conditions (LD WT-GFP and
431 HD Δ*dotA*-GFP (Fig S8B, C).
432 Taken together, our results suggest that MyD88 signalling is not required for the innate
433 immune response against *L. pneumophila* infection in the zebrafish larvae, similar to what is seen in
434 human cell infection models. However, MyD88 signalling may also be functionally compensated by
435 other immune signalling pathways.
436
437 **DISCUSSION**
438 In this study, we developed a zebrafish larva infection model for *L. pneumophila* and have analysed
439 host pathogen interactions as well as the host innate immune response to infection. We have found
440 that a successful infection of zebrafish larvae by *L. pneumophila* depends on the infection site, the
441 infection dose, the T4SS Dot/Icm and the innate immune response of the host, in particular on the

442 action of macrophages and neutrophils. Wild type zebrafish larvae are susceptible to infection in a
443 dose dependent manner, as larvae injected in the bloodstream with increasing doses of bacteria
444 developed an infection with bacterial dissemination and replication, concomitant with host death
445 proportional to the initial injected bacterial load. However, the fact that only about 30% of the larvae
446 displayed this phenotype, indicates that the innate immune defence of the larvae against
447 *L. pneumophila* infection is relatively efficient. Thus, the establishment of infection is determined not
448 only by the infection dose but also by the capacity of the host immune system to quickly and
449 efficiently fence off the infection.

450 Like in several other zebrafish infection models, only blood borne bacteria can proliferate
451 and induce mortality in zebrafish larvae (Emma do you have some papers we could cite?). Once in
452 the blood circulation, bacteria are engulfed and are eliminated by both macrophages and neutrophils
453 in a dose-dependent manner. However, T4SS competent *L. pneumophila* are also able to reach the
454 yolk region, cross the endothelium of the yolk vessels and enter the yolk sac region. Once there,
455 *L. pneumophila* gains a significant advantage in the pathogen-host arms race and establishes a
456 replicative niche where it proliferates extensively, forming complex, aggregated bacterial structures,
457 located below and above the yolk cell membrane, that professional phagocytes fail to clear. In the
458 yolk sac region *L. pneumophila* is protected from the host immune system, when it reaches the yolk
459 cell, as professional phagocytes are unable to enter in the yolk. Extensive proliferation of the bacteria
460 eventually leads to host death, likely due to exhaustion of the nutrients present in the yolk, which are
461 key in supporting the larvae development. Interestingly, we have also observed that in few cases
462 (less than 5%) the infected larvae were able to extrude the bacterial aggregates growing in the yolk
463 and survived. This host defence mechanism has also been reported in a caudal fin model of
464 *Mycobacterium marinum* infection, where infected zebrafish larvae extruded the bacteria-containing
465 granuloma and during infection with *Aspergillus fumigatus* [45, 46] .

466 To our knowledge, the tropism, and the establishment of a replicative niche in the yolk upon
467 pathogen injection in the bloodstream is a unique feature of *L. pneumophila.* Our results have shown
468 that, when macrophages and neutrophils are depleted, blood-borne *L. pneumophila* can still reach
469 the yolk cell. It seems that *L. pneumophila* can cross the venous endothelium of the yolk and reach
470 the nutrient-rich content of the yolk cell. Interestingly, direct yolk cell injection revealed that also
471 only the WT but not the T4SS knockout strain is able to replicate and establish a persistent infection
472 in the yolk, irrespective of the dose injected. This result points towards the involvement of the T4SS
473 system and its secreted effectors in infection and replication but also nutrient uptake in the yolk
474 environment. Yolk sac injection has already been used previously for the analyses of *Candida*
475 *albicans* infection or the study of streptococcal infections, however in this case the pathogens
476 disseminated from the yolk sac into the animal [47, 48], a phenotype not observed when

477 *L. pneumophila* was injected in the yolk sac. Further analyses of the phenotype of yolk sac
478 replication in embryonated chicken eggs showed again that only WT *L. pneumophila* can replicate in
479 the yolk region, further supporting the importance of the T4SS in nutrient uptake in addition to its
480 known role in infection (Fig. S5A, B, C). *L. pneumophila* is known to mainly use amino acids as carbon
481 and energy sources for growth [49] and secreted T4SS effectors have been shown to aid in amino
482 acid uptake [50]. However, fatty acids, glucose and/or glycerol also serve as carbon sources during
483 the later stages of the life cycle of *L. pneumophila* [51, 52], but effectors connected to the uptake of
484 these nutrients have not been identified yet. The yolk cell is composed of a complex and dynamic
485 mixture of different lipids on which the zebrafish larvae rely on for nutrition throughout
486 development in the early larva phase. Cholesterol and phosphatidylcholine are the main constituents
487 until 120hpf, with triacylglycerol, phosphatidylinositol, phosphatidylethanolamine, diacyl-glycerol,
488 cholesteryl esters and sphingomyelins also present in significant concentrations [53]. *L. pneumophila*
489 is known to secrete several effectors with lipolytic activity through its T4SS which could be important
490 for growth in a lipid rich environment like the yolk [54]. In a first attempt to identify one of these
491 effectors we analysed the growth of a *L. pneumophila* mutant for a gene encoding a sphingosine-1
492 phosphate lyase (*Lp*Spl) [27]. When compared to the WT strain after direct injection in the zebrafish
493 larvae yolk sac a small but significant difference in larvae mortality was observed for the Δ*spl* strain,
494 suggesting that *Lp*Spl is one of several effectors that might participate in nutrient acquisition from
495 lipids (Fig. S5A). However, further analyses are needed to characterize the involvement of *Lp*Spl in
496 nutrient acquisition during infection of the yolk region and to identify other effectors potentially
497 implicated in this phenotype.
498 Studies of *Legionella* infection in humans, guinea pigs and mouse lungs have shown that
499 *L. pneumophila* interacts closely with neutrophils and mononuclear phagocytes [55, 56]. Professional
500 phagocytes are the main replication niche for *L. pneumophila* with monocytes and macrophages, and
501 in particular alveolar macrophages, representing the main cells for replication in the lungs [57-60]. *In*
502 *vivo* studies in mice have shown that upon lung infection with *L. pneumophila* neutrophils, cDCs,
503 monocytes, and monocyte-like cells are rapidly recruited to the infection site, but although all these
504 cells seem to engulf the bacteria, *L. pneumophila* can only translocate effectors into neutrophils and
505 alveolar macrophages. In zebrafish macrophages appear during the first days of development,
506 followed by neutrophils a day later, with both forming an efficient immune system that protects the
507 developing fish [25, 61-63]. Therefore, the zebrafish larva offers a unique possibility to interrogate
508 the role of innate immune responses to infection [23]. Indeed, macrophage depleted larvae showed
509 a dramatically increased susceptibility to *L. pneumophila* infection as nearly 100% of larvae
510 inoculated with HD of WT and 30% of larvae inoculated with LD of *L. pneumophila* died from the
511 infection. Hence, macrophages are the first line of infection control against *L. pneumophila* and are

512 essential for restricting and controlling blood-borne infections, similar to what was observed for
513 *Burkholderia cenocepacia or Staphylococcus aureus* zebrafish infection [64, 65]. In contrast, when
514 neutrophils were depleted, the innate immune response was less affected, suggesting that
515 neutrophils are also required to ensure an effective innate immune response and, that macrophages
516 alone are not able to contain high burdens of *L. pneumophila* infection (Fig. 6).
517 Human innate immune signalling relies strongly on activation of Toll-like receptors (TLRs) and
518 respective adaptor molecules, all of which are highly conserved in the zebrafish [66, 67]. One of
519 these adaptors is MyD88, known as a central player in interleukin 1 receptor (IL-1R) and TLR
520 signalling in humans and mammalian models [68]. MyD88 signalling is crucial for mice to combat
521 *L. pneumophila* infection, as it triggers the early secretion of inflammatory cytokines, neutrophil
522 recruitment, and the host immune response to the infection. Consequently, mice that lack MyD88
523 are highly susceptible to infection [39-42]. However, in MyD88 depleted human macrophages
524 *L. pneumophila* replication is not different to replication in WT cells [44] Here we show, Myd88
525 signalling does not play a crucial role or may be redundant in the control of the innate immune
526 response to *L. pneumophila* infection of zebrafish larvae, suggesting that zebrafish infection mirrors
527 human infection better than the mouse model. In the mouse model infected macrophages are
528 incapable of producing cytokines, such as tumour necrosis factor (TNF) and interleukin-12 (IL-12),
529 which are necessary to control infection. In contrast, infection of zebrafish larvae with WT *L.*
530 *pneumophila* induced a rapid (by 6hpi) and robust induction of *il1b* and *tnfa* gene expression.
531 However, it is thought that IL-1 released initially by *L. pneumophila*-infected macrophages drives the
532 production of critical cytokines by bystander cells [37]. Infection of zebrafish larvae with HD of WT
533 *L. pneumophila* induced a rapid (by 6hpi) and robust induction of *il1b* and *tnfa* gene expression
534 whereas WT LD infection leads only to a short induction of *Il1b* transcript levels at 6hpi before
535 declining to CTRL levels at later time points, suggesting that a short boost of IL-1β is sufficient to
536 control LD of *L. pneumophila*. However, for a high load of *L. pneumophila* even a high and long-term
537 induction of IL-1β is not sufficient to warrant infection control, suggesting that the self-regulation of
538 the immune response may be abrogated leading to a constant activation of IL-1β expression.
539 Moreover, gene expression analyses also confirms that Myd88 has no influence on the control of the
540 inflammatory response, as no statistically significant difference in the transcript levels of *il1b*, *tnfa,*
541 *ifng1 or infg2* was observed further suggesting that activation of the IL1R and certain TLR pathways
542 are not crucial for *L. pneumophila* clearance in zebrafish larvae. It is even possible that IL-1β release
543 is beneficial for *L. pneumophila* replication, as it was shown that IL-1β may also indicate an activation
544 of the metabolic state of the bystander cells as it was shown that IL-1β induces a shift towards more
545 metabolically active cells and increased cellular glucose uptake [69], which could aid *L. pneumophila*
546 replication.

547 In conclusion, the zebrafish infection model for *L. pneumophila* mimics the immune response
548 known of human infection and recalls the essentiality of the type IV secretion system for virulence of
549 this pathogen. The unique advantages of the zebrafish model provide now exciting possibilities to
550 further explore *L. pneumophila* host interactions and to interrogate at the molecular level the
551 bacterial determinants and host factors involved in the dynamics of bacterial dissemination, the
552 molecular basis of yolk region invasion and the interactions of the bacteria with macrophages and
553 neutrophils.
554
555 **MATERIALS AND METHODS**
556
557 **Ethics Statement.** Animal experiments were performed according to European Union guidelines for
558 handling of laboratory animals
559 (http://ec.europa.eu/environment/chemicals/lab_animals/home_en.htm) and were approved by the
560 Institut Pasteur Animal Care and Use Committee. and the French Ministry of Research
561 (APAFIS#31827). The inoculation of embryonated chicken eggs is a standard procedure in diagnostics
562 for multiplication and antigen production of *Legionella* and is not covered by the national law for
563 animal experiments in France (Décret n° 2013-118 du 1er février 2013).
564
565 **Zebrafish care and maintenance.** Wild-type AB fish, initially obtained from the Zebrafish
566 International Resource Center (Eugene, OR), Tg(*Lyz::DsRed)*^{nz50} [70], Tg*(mfap4::mCherryF*) (ump6Tg)
567 [36] Tg(mpx:GFP)^{i114} [71] , Tg(kdrl::mCherry)^{is5} [72] and *myd88*^{hu3568} mutant line (obtained from the
568 Hubrecht Laboratory and the Sanger Institute Zebrafish Mutation Resource) [73], were raised in our
569 facility. Eggs were obtained by natural spawning, bleached according to standard protocols, and kept
570 in Petri dishes containing Volvic source water and, from 24 hours post fertilization (hpf) onwards
571 0.003% 1-phenyl-2-thiourea (PTU) (Sigma-Aldrich) was added to prevent pigmentation. Embryos
572 were reared at 28°C or 24°C according to the desired speed of development; infected larvae were
573 kept at 28°C. Timings in the text refer to the developmental stage at the reference temperature of
574 28.5°C. Larvae were anesthetized with 200µg/ml tricaine (Sigma-Aldrich) during the injection
575 procedure as well as during *in vivo* imaging and processing for bacterial burden evaluation or
576 cytokine expression studies.
577
578 **Bacterial strains and growth conditions.** *Legionella pneumophila* strain Paris carrying the pNT28
579 plasmid encoding for green fluorescent protein (constitutive GFP) [74], wild-type (WT-GFP) or Δ*dotA*-
580 GFP were plated from -80°C glycerol stocks on N-(2-acetamido)-2-aminoethanesulfonic acid (ACES)-
581 buffered charcoal yeast-extract (BCYE) medium supplemented with 10 µg/ml of chloramphenicol and

582 cultured for 3 days at 37°C. Suspensions were prepared by resuspending bacteria in sterile 1x
583 Phosphate Buffered Saline (PBS) and adjusting the OD 600 according to the desired bacterial
584 concentrations for injection.
585
586 **Morpholino injections**. Morpholino antisense oligonucleotides (Gene Tools LLC, Philomath, OR, USA)
587 were injected at the one to two cell stage as described [75]. A low dose (4ng) of *spi1b* (previously
588 named pu1) translation blocking morpholino (GATATACTGATACTCCATTGGTGGT) [76] blocks
589 macrophage development only but can also block neutrophil development when it is injected at a
590 higher dose (20ng in 2nl). The csf3r translation blocking morpholino
591 (GAACTGGCGGATCTGTAAAGACAAA) (4ng) [34] was injected to block neutrophil development.
592 Control morphants were injected with 4ng control morpholino, with no known target
593 (GAAAGCATGGCATCTGGATCATCGA).
594
595 **Amoebae infections.** *Acanthamoebae castellanii* was infected with *L. pneumophila* wild type
596 expressing GFP and then used to assess if zebrafish develop an infection when ingesting infected
597 amoebae. *A. castellanii* was seeded in a flask with infection buffer (4 mM $MgSO_4$, 0.4 M $CaCl_2$, 0.1%
598 sodium citrate dihydrate, 0.05 mM $Fe(NH_4)_2(SO_4)_2 \times 6H_2O$, 2.5 mM NaH_2PO_3, 2.5 mM K_2HPO_3), and
599 after 1 hour of attachment the cells were infected with the bacteria at MOI 1. After one hour of
600 infection, the amoebae were washed three times with PBS and fresh infection buffer was added.
601 After 48 hours of infection, the amoebae were carefully washed, detached, and used for the bath
602 immersion experiment.
603
604 **Bath immersion.** Experiments were performed using the AB or Tg(mfap4::mCherryF) zebrafish lines
605 maintained at 28 °C under standard conditions in Volvic water. Bath immersion infections were done
606 with 120hpf larvae that already had a developed swim bladder. Groups of 10 larvae were distributed
607 into 6-well plates containing 4.0 ml/well of Volvic spring water and either 1ml of bacterial
608 suspension, 1ml of *L. pneumophila*-containing amoebae, or 1ml of non-infected amoebae, all in PBS.
609 The plates were incubated at 28 °C for 24 hours, and then larvae were individually distributed in an
610 individual well in 24 wells culture plates and monitored by imaging using a fluorescence
611 stereomicroscope.
612
613 **Zebrafish injection.** The volume of injected suspension was deduced from the diameter of the drop
614 obtained after mock microinjection, as described in [75]. Bacteria were recovered by centrifugation,
615 washed, resuspended at the desired concentration in PBS. 72h post-fertilization (hpf) anesthetized
616 zebrafish larvae were microinjected iv or in closed cavities, or the yolk with 0.5-1nl of bacterial

617 suspension at the desired dose (~10^3 bacteria/nl for Low Dose (LD) and ~10^4 bacteria/nl for High
618 Dose (HD) as described [24, 32]. Infected larvae were transferred into individual wells (containing
619 1ml of Volvic water + 0.003% PTU in 24-well culture plates), incubated at 28°C and regularly observed
620 under a stereomicroscope, twice a day overtime up to 72hpi.
621
622 **Evaluation of the bacterial burden in infected larvae.** The bacterial burden was measured routinely
623 by counting the total number of fluorescent pixels corresponding to the GFP channel using the
624 Metavue software 7.5.6.0. Briefly, images corresponding to the GFP channel were adjusted to a fixed
625 threshold that allowed to abrogate the background of the autofluorescence of the yolk. The same
626 threshold was used for all images. The histogram in the "Analyze" menu was used to obtain the
627 number of black and white pixels. As shown in figure S1A, the percentage of white pixels in each
628 image corresponding to *L. pneumophila* was plotted using GraphPad Prism® software. This method
629 was chosen to routinely quantify bacterial burden as it allows to follow each infected larva overtime
630 (individual larvae were imaged with the fluorescence stereomicroscope daily using the same settings
631 from 0 to 72hpi).
632
633 **Bacterial burden analyses by FACS**. Injected zebrafish larvae were collected at 0, 24, 48 and 72hpi
634 and lysed. Each larva was placed in a 1.5 ml Eppendorf tube and anesthetized with tricaine
635 (200µg/ml), washed with 1ml of sterile water and placed in 150 µl of sterile water. Larvae were then
636 homogenized using a pestle motor mixer (Argos). Each sample was transferred to an individual well
637 of a 96 well plate, counted on a MACSQuant VYB FACS (Miltenyi Biotec) and data analysed using
638 FlowJo version 7.6.5. as shown in Figure S1B. For CFU enumeration, serial dilutions were plated on
639 BCYE agar plates supplemented with10ug/ml chloramphenicol and the *Legionella* Selective
640 Supplement GVPN (Sigma) added according to the manufacturer's instructions. Plates were
641 incubated for 4-5 days at 37°C and colonies with the appropriate morphology and colour were scored
642 using the G-Box imaging system (Syngene) and enumerated using the Gene Tools software (Syngene)
643 as shown in Figure S1C. Manual quantification was also performed to identify absolute absence or
644 presence of bacteria in the different zebrafish compartments. Larvae with a single GFP dot
645 (indicating the presence of few bacteria) were considered as infected. The resulting statistical
646 presence map was used to follow the evolution of the infection and dissemination of *L. pneumophila*
647 in zebrafish larvae over time (Figure 1E).
648
649 **Inoculation and quantification of *L. pneumophila* strains in *in ovo* experiments.** Fertilized chicken
650 eggs purchased from a local producer (Saint-Maurice-sur-Dargoire, Rhône, France) were incubated at
651 35°C in an egg incubator (Maino, Italy) to maintain normal embryonic development. Eggs were

652 pathogen and antibiotic free. On day 0, 23 embryonated chicken eggs (ECE) were inoculated at 8
653 days of embryonation (DOE) with either *L. pneumophila* WT (n=9), *L. pneumophila ΔdotA* (n=7) or
654 sterile PBS as control (n=7). *L. pneumophila* concentration in WT and Δ*dotA* suspensions before ECE
655 injection was quantified at 9.2 $\log_{10}$ CFU/mL and 9.1 $\log_{10}$ CFU/mL, respectively. *L. pneumophila*
656 concentration in the yolk sac of ECE directly after injection were estimated, considering both the
657 measured inoculum counts and the yolk sac volumes (median (interquartile range) [IQR] volume, 30
658 [28.7-31.2] mL), at 7.4 and 7.3 $\log_{10}$ CFU/mL in the WT and Δ*dotA* groups, respectively. Two-day
659 cultures of Lpp-WT and Lpp-Δ*dotA* on BCYE at 36°C were suspended in PBS at a DO = 2.5 McFarland
660 (9 $\log_{10}$ CFU/mL) and 0.5 mL of suspensions or PBS (negative control) were inoculated in the yolk sac
661 of ECE. After inoculation, ECE were candled every 24 hours to assess embryo viability until day-6 post
662 infection. Embryos that died the day after inoculation (n=2, corresponding to one WT-infected and
663 one *ΔdotA*-infected embryo) were discarded for *L. pneumophila* quantification as death was probably
664 due to bad inoculation. Dead embryos were stored at 4°C overnight prior to harvesting the yolk sacs.
665 Remaining live embryos at 6-days post injection were euthanized by overnight refrigeration and the
666 yolk sacs were collected. After measuring their volume, yolk sacs were homogenized using
667 gentleMACS™ Octo Dissociator (Miltenyi Biotec, Germany) and 100 µL of serial dilutions at 10^{-2}, 10^{-4}
668 and 10^{-6} were automatically plated using easySpiral® automatic plater (Interscience, France) in
669 triplicates on BCYE agar. *L. pneumophila* were quantified after 5 days-incubation using Scan® 1200
670 Automatic HD colony counter (Interscience, France). Comparison of survival curves was performed
671 using Log-rank (Mantel-Cox) test. $P < 0.05$ was considered statistically significant. Comparison of *L.*
672 *pneumophila* quantifications between WT- and Δ*dotA*-infected embryos was done using Mann-
673 Whitney test. $P < 0.05$ was considered statistically significant (symbols: **** $P < 0.0001$; ***$P <$
674 0.001; **$P < 0.01$; *$P < 0.05$).
675
676 **Live imaging, image processing and analysis.** Quantification of total neutrophils and/or macrophages
677 on living transgenic reporter larvae upon infection was performed as previously described [32].
678 Briefly, bright field, DsRed and GFP images of whole living anesthetized larvae were taken using a
679 Leica Macrofluo™ Z16 APOA (zoom 16:1) equipped with a Leica PlanApo 2.0X lens, and a
680 Photometrics® CoolSNAP™ *HQ2* camera. Images were captured using Metavue software 7.5.6.0
681 (MDS Analytical Technologies). Then larvae were washed and transferred in a new 24 wells plate
682 filled with 1ml of fresh Volvic water per well, incubated at 28°C and imaged again under the same
683 conditions the day after. Pictures were analysed, and Tg(*lyzC::DsRed*) neutrophils or
684 Tg(*mfap4::mCherryF*) macrophages manually counted using the ImageJ software (V 1.52a). Counts
685 shown in figures are numbers of cells per image. The quantification of fluorescence images was also

686 done using CellProfiler™ Software (Broad Institute) using two semi-automatic batch pipelines. Both
687 pipelines normalize the intensity, operate image pre-processing, and use thresholding to calculate
688 the percentage of area positive for macrophage/neutrophils and bacteria, normalized on the whole
689 image area. Both pipelines also take advantage of manual editing to increase identification accuracy
690 and define the yolk area. The positive signal is then automatically masked to calculate the amount of
691 signal in the body or yolk of each zebrafish for all the experiments and produce a .csv file used for
692 subsequent statistical treatment (Figure 3F and Figure S6). High resolution confocal live imaging of
693 injected larvae was performed as previously described [77]. Briefly, injected larvae were positioned
694 in lateral or ventral position in 35 mm glass-bottom-Dishes (Ibidi Cat#: 81158) or in glass bottom-
695 8well-slides (Ibidi Cat#: 80827). Larvae were immobilized using a 1% low-melting-point agarose
696 (Promega; Cat#: V2111) solution and covered with Volvic water containing tricaine. A Leica SP8
697 confocal microscope equipped with two PMT and Hybrid detector, a 10X dry (PL Fluotar 10X
698 dry:0.30), 20X IMM (HC PL APO CS2 20X/0.75), or a 40x water IMM (HC PL APO CS2 40X/1.10)
699 objective, a X–Y motorized stage and with LAS-X software, was used to live image injected larvae. To
700 generate images of the whole larvae, a mosaic of confocal z-stack of images was taken with the 10X
701 or 20X objective using the Tile Scan tool of the LAS-X software and was stitched together using the
702 Mosaic Merge tool of the LAS-X software. All samples were acquired using the same settings,
703 allowing comparisons of independent experiments. The acquisitions were post processed with the
704 Lightning tool of the LAS-X software to eliminate noise (deconvolution). After acquisition, larvae were
705 washed and transferred in a new 24-well plate filled with 1 ml of fresh Volvic water per well,
706 incubated at 28°C and imaged again under the same conditions over time. A Leica SPE inverted
707 confocal microscope and a 40x oil IMM objective (ACS APO 40 × 1.15 UV) was also used to live image
708 larvae infected with *L. pneumophila* Δ*dotA*-GFP (Fig 4, 5). The 3D or 4D files generated by the time-
709 lapse acquisitions were processed, cropped, analysed, and annotated using the LAS-X and LAS-AF
710 Leica software. Acquired Z-stacks were projected using maximum intensity projection and exported
711 as AVI files. Frames were captured from the AVI files and handled with Miocrosoft PowerPoint ®
712 (Microsoft Office 365) software to mount figures. AVI files were cropped and annotated using ImageJ
713 software. Files generated with the LAS-X software were also processed and analysed with the Imaris
714 software version9.5 (Bitplane, OXFORD Instruments) for 3D or 4D reconstruction, surfacing and
715 volume rendering. The yolk region has been manually annotated (Movie S5).
716
717 **qRT-PCR to measure gene expression of cytokine encoding genes.** RNA was extracted from
718 individual larvae using the RNeasy® Mini Kit (Qiagen). cDNA was obtained using M-MLV H- reverse-
719 transcriptase (Promega) with a dT_{17} primer. Quantitative PCR was performed on an ABI7300

720 thermocycler (Applied Biosystems) using TakyonTM ROX SYBR® 2X MasterMix (Eurogentec) in a final
721 volume of 10 µl. Primers used: *ef1a (housekeeping gene used for normalization):*
722 GCTGATCGTTGGAGTCAACA and ACAGACTTGACCTCAGTGGT*; il1b*: GAGACAGACGGTGCTGTTTA and
723 GTAAGACGGCACTGAATCCA*; tnfa*: TTCACGCTCCATAAGACCCA and CAGAGTTGTATCCACCTGTTA*; ifng-*
724 *1-1*: ACCAGCTGAATTCTAAGCCAA and TTTTCGCCTTGACTGAGTGAA; *ifng-2:* GAATCTTGAGGAAAGTG
725 AGCA and TCGTTTTCCTTGATCGCCCA
726 **Statistical analysis.** Normal distributions were analysed with the Kolmogorov– Smirnov and the
727 Shapiro–Wilk tests. To evaluate difference between means of normally distributed data (for
728 neutrophil and macrophage numbers), an analysis of variance followed by Bonferroni's multiple
729 comparison tests was used. For bacterial burdens (CFU/FACS counts), values were Log10
730 transformed. For cytokine expression and bacterial burdens (evaluated by
731 fluorescent pixel count, or FACS) non-Gaussian data were analysed with the Kruskal–Wallis test
732 followed by Dunn's multiple comparison test. $P < 0.05$ was considered statistically significant
733 (symbols: **** $P < 0.0001$; ***$P < 0.001$; **$P < 0.01$; *$P < 0.05$). No symbol on graphs means that not
734 statistically differences were observed. Survival data were plotted using the Kaplan–Meier estimator
735 and log-rank (Mantel–Cox) tests were performed to assess differences between groups. Statistical
736 analyses were performed using GraphPad Prism® software. Statistical analyses for *in ovo*
737 experiments, were performed using GraphPrism version 9.4.
738
739 **Author contributions**
740 FV, LB, SJ, ECG and CB designed the experiments. FV, LB, VL, DS, MI and ECG performed the
741 experiments. FV, LB, VL, ECG analysed the experiments. FV drafted, and ECG and CB wrote the
742 manuscript with input from all authors. ECG and CB supervised the work and acquired funds.
743
744 **Data Availability:** All relevant data are within the paper and its Supporting Information files. The
745 movies related to the paper are available at https://zenodo.org/deposit/7410466
746 **Competing Interest**
747 The authors declare there are no competing interests.
748
749 **ACKNOWLEDGEMENTS**
750 We thank Pedro Escoll and Jean-Pierre Levraud for help and ideas in the initial set up of the project
751 and Tobias Sahr for critical reading and helpful discussions, Philippe Herbomel for helpful scientific
752 advice, and Yohann Rolin for his excellent care of the fish. Work in the CB laboratory is financed by
753 the Institut Pasteur, the Fondation pour la Recherche Médicale (FRM) grant EQU201903007847 and

754 the grant ANR-10-LABX-62-IBEID and ANR-22-CE15 0009 01 ZebraLegion. Work in ECG group is
755 financed by Institut Pasteur, CNRS, and ANR 17-CE15-0026 and 20-CE15-0024 and ANR-22-CE15 0009
756 01 ZebraLegion. Valerio Laghi is funded by ANR 20-CE15-0024. We acknowledge the Image analyses
757 Hub at Institut Pasteur for the use of the IMARIS workstation. The funders, other than the authors,
758 did not play any role in the study or in the preparation of the article or decision to publish.
759

760 **REFERENCES**

761 1. Fliermans CB. Ecology of Legionella: From Data to Knowledge with a Little Wisdom. Microb Ecol.
762 1996;32(2):203-28. PubMed PMID: 8688009.
763 2. Cunha BA, Burillo A, Bouza E. Legionnaires' disease. Lancet. 2016;387(10016):376-85. doi:
764 10.1016/S0140-6736(15)60078-2. PubMed PMID: 26231463.
765 3. Rowbotham TJ. Preliminary report on the pathogenicity of *Legionella pneumophila* for freshwater
766 and soil amoebae. J Clin Pathol. 1980;33(12):1179-83.
767 4. Boamah DK, Zhou G, Ensminger AW, O'Connor TJ. From Many Hosts, One Accidental Pathogen:
768 The Diverse Protozoan Hosts of *Legionella*. Frontiers in cellular and infection microbiology.
769 2017;7:477. doi: 10.3389/fcimb.2017.00477. PubMed PMID: 29250488; PubMed Central PMCID:
770 PMCPMC5714891.
771 5. Mampel J, Spirig T, Weber SS, Haagensen JA, Molin S, Hilbi H. Planktonic replication is essential
772 for biofilm formation by *Legionella pneumophila* in a complex medium under static and dynamic
773 flow conditions. Appl Environ Microbiol. 2006;72(4):2885-95. doi: 10.1128/AEM.72.4.2885-
774 2895.2006. PubMed PMID: 16597995; PubMed Central PMCID: PMC1448985.
775 6. McDade JE, Shepard CC, Fraser DW, Tsai TR, Redus MA, Dowdle WR. Legionnaires' disease:
776 isolation of a bacterium and demonstration of its role in other respiratory disease. N Engl J Med.
777 1977;297(22):1197-203.
778 7. Lanternier F, Ader F, Pilmis B, Catherinot E, Jarraud S, Lortholary O. Legionnaire's Disease in
779 Compromised Hosts. Infect Dis Clin North Am. 2017;31(1):123-35. Epub 2017/02/06. doi:
780 10.1016/j.idc.2016.10.014. PubMed PMID: 28159172.
781 8. Naujoks J, Lippmann J, Suttorp N, Opitz B. Innate sensing and cell-autonomous resistance
782 pathways in *Legionella pneumophila* infection. Int J Med Microbiol. 2018;308(1):161-7. Epub
783 2017/11/04. doi: 10.1016/j.ijmm.2017.10.004. PubMed PMID: 29097162.
784 9. Isberg RR, O'Connor TJ, Heidtman M. The *Legionella pneumophila* replication vacuole: making a
785 cosy niche inside host cells. Nat Rev Microbiol. 2009;7(1):13-24. Epub 2008/11/18. doi:
786 nrmicro1967 [pii]10.1038/nrmicro1967. PubMed PMID: 19011659.
787 10. Mondino S, Schmidt S, Rolando M, Escoll P, Gomez-Valero L, Buchrieser C. Legionnaires' Disease:
788 State of the Art Knowledge of Pathogenesis Mechanisms of *Legionella*. Annu Rev Pathol.
789 2020;15:439-66. Epub 2019/10/29. doi: 10.1146/annurev-pathmechdis-012419-032742. PubMed
790 PMID: 31657966.
791 11. Ensminger AW. *Legionella pneumophila*, armed to the hilt: justifying the largest arsenal of
792 effectors in the bacterial world. Curr Opin Microbiol. 2016;29:74-80. doi:
793 10.1016/j.mib.2015.11.002. PubMed PMID: 26709975.
794 12. Cazalet C, Rusniok C, Bruggemann H, Zidane N, Magnier A, Ma L, et al. Evidence in the *Legionella*
795 *pneumophila* genome for exploitation of host cell functions and high genome plasticity. Nat
796 Genet. 2004;36(11):1165-73.
797 13. Mondino S, Schmidt S, Buchrieser C. Molecular Mimicry: a Paradigm of Host-Microbe Coevolution
798 Illustrated by Legionella. mBio. 2020;11(5). Epub 2020/10/08. doi: 10.1128/mBio.01201-20.
799 PubMed PMID: 33024033.

14. Brassinga AK, Kinchen JM, Cupp ME, Day SR, Hoffman PS, Sifri CD. *Caenorhabditis* is a metazoan host for *Legionella*. Cell Microbiol. 2009;12(3):343-61. Epub 2009/10/30. doi: CMI1398 [pii]10.1111/j.1462-5822.2009.01398.x. PubMed PMID: 19863556.
15. Harding CR, Schroeder GN, Reynolds S, Kosta A, Collins JW, Mousnier A, et al. *Legionella pneumophila* pathogenesis in the *Galleria mellonella* infection model. Infect Immun. 2012;80(8):2780-90. doi: 10.1128/IAI.00510-12. PubMed PMID: 22645286; PubMed Central PMCID: PMC3434583.
16. Brown AS, van Driel IR, Hartland EL. Mouse Models of Legionnaires' Disease. Curr Top Microbiol. 2014;376:271-91. doi: 10.1007/82_2013_349. PubMed PMID: WOS:000330592900014.
17. Breiman RF, Horwitz MA. Guinea pigs sublethally infected with aerosolized *Legionella pneumophila* develop humoral and cell-mediated immune responses and are protected against lethal aerosol challenge. A model for studying host defense against lung infections caused by intracellular pathogens. J Exp Med. 1987;165(3):799-811. PubMed PMID: 3819647.
18. Weeratna R, Stamler DA, Edelstein PH, Ripley M, Marrie T, Hoskin D, et al. Human and guinea pig immune responses to Legionella pneumophila protein antigens OmpS and Hsp60. Infect Immun. 1994;62(8):3454-62. PubMed PMID: 7913699.
19. Akhter A, Gavrilin MA, Frantz L, Washington S, Ditty C, Limoli D, et al. Caspase-7 activation by the Nlrc4/Ipaf inflammasome restricts *Legionella pneumophila* infection. PLoS Pathog. 2009;5:e1000361. doi: doi: 10.1371/journal.ppat.1000361.
20. Santic M, Asare R, Doric M, Abu Kwaik Y. Host-dependent trigger of caspases and apoptosis by *Legionella pneumophila*. Infect Immun. 2007;75(6):2903-13.
21. Masud S, Torraca V, Meijer AH. Modeling Infectious Diseases in the Context of a Developing Immune System. Curr Top Dev Biol. 2017;124:277-329. doi: 10.1016/bs.ctdb.2016.10.006. PubMed PMID: WOS:000406859900009.
22. Torraca V, Mostowy S. Zebrafish Infection: From Pathogenesis to Cell Biology. Trends in Cell Biology. 2018;28(2):143-56. doi: 10.1016/j.tcb.2017.10.002. PubMed PMID: WOS:000424633500006.
23. Gomes MC, Mostowy S. The Case for Modeling Human Infection in Zebrafish. Trends in Microbiology. 2020;28(1):10-8. doi: 10.1016/j.tim.2019.08.005. PubMed PMID: WOS:000503037700005.
24. Colucci-Guyon E, Tinevez JY, Renshaw SA, Herbomel P. Strategies of professional phagocytes in vivo: unlike macrophages, neutrophils engulf only surface-associated microbes. J Cell Sci. 2011;124(Pt 18):3053-9. Epub 2011/08/27. doi: 10.1242/jcs.082792. PubMed PMID: 21868367.
25. Herbomel P, Thisse B, Thisse C. Ontogeny and behaviour of early macrophages in the zebrafish embryo. Development. 1999;126(17):3735-45. Epub 1999/08/06. PubMed PMID: 10433904.
26. Hilbi H, Buchrieser C. Microbe Profile: *Legionella pneumophila* - a copycat eukaryote. Microbiology (Reading). 2022;168(3). doi: 10.1099/mic.0.001142. PubMed PMID: 35230931.
27. Rolando M, Escoll P, Nora T, Botti J, Boitez V, Bedia C, et al. *Legionella pneumophila* S1P-lyase targets host sphingolipid metabolism and restrains autophagy. Proc Natl Acad Sci U S A. 2016;113(7):1901-6. doi: 10.1073/pnas.1522067113. PubMed PMID: 26831115; PubMed Central PMCID: PMCPMC4763766.
28. Liu X, Shin S. Viewing *Legionella pneumophila* Pathogenesis through an Immunological Lens. J Mol Biol. 2019;431(21):4321-44. Epub 2019/07/29. doi: 10.1016/j.jmb.2019.07.028. PubMed PMID: 31351897.
29. Cohen SB, Gern BH, Delahaye JL, Adams KN, Plumlee CR, Winkler JK, et al. Alveolar Macrophages Provide an Early *Mycobacterium tuberculosis* Niche and Initiate Dissemination. Cell Host Microbe. 2018;24(3):439-46 e4. Epub 2018/08/28. doi: 10.1016/j.chom.2018.08.001. PubMed PMID: 30146391; PubMed Central PMCID: PMCPMC6152889.
30. Mengue L, Richard FJ, Caubet Y, Rolland S, Hechard Y, Samba-Louaka A. *Legionella pneumophila* decreases velocity of Acanthamoeba castellanii. Exp Parasitol. 2017;183:124-7. Epub 2017/08/06. doi: 10.1016/j.exppara.2017.07.013. PubMed PMID: 28778742.

31. Simon S, Wagner MA, Rothmeier E, Muller-Taubenberger A, Hilbi H. Icm/Dot-dependent inhibition of phagocyte migration by *Legionella* is antagonized by a translocated Ran GTPase activator. Cell Microbiol. 2014;16(7):977-92. doi: 10.1111/cmi.12258. PubMed PMID: 24397557.
32. Mostowy S, Boucontet L, Mazon Moya MJ, Sirianni A, Boudinot P, Hollinshead M, et al. The zebrafish as a new model for the in vivo study of *Shigella flexneri* interaction with phagocytes and bacterial autophagy. PLoS Pathog. 2013;9(9):e1003588. doi: 10.1371/journal.ppat.1003588. PubMed PMID: 24039575; PubMed Central PMCID: PMCPMC3764221.
33. Su F, Juarez MA, Cooke CL, Lapointe L, Shavit JA, Yamaoka JS, et al. Differential regulation of primitive myelopoiesis in the zebrafish by Spi-1/Pu.1 and C/ebp1. Zebrafish. 2007;4(3):187-99. Epub 2007/11/29. doi: 10.1089/zeb.2007.0505. PubMed PMID: 18041923.
34. Ellett F, Pase L, Hayman JW, Andrianopoulos A, Lieschke GJ. mpeg1 promoter transgenes direct macrophage-lineage expression in zebrafish. Blood. 2011;117(4):e49-56. Epub 2010/11/19. doi: 10.1182/blood-2010-10-314120. PubMed PMID: 21084707; PubMed Central PMCID: PMCPMC3056479.
35. Palha N, Guivel-Benhassine F, Briolat V, Lutfalla G, Sourisseau M, Ellett F, et al. Real-time whole-body visualization of Chikungunya Virus infection and host interferon response in zebrafish. PLoS Pathog. 2013;9(9):e1003619. Epub 2013/09/17. doi: 10.1371/journal.ppat.1003619. PubMed PMID: 24039582; PubMed Central PMCID: PMCPMC3764224.
36. Phan QT, Sipka T, Gonzalez C, Levraud JP, Lutfalla G, Mai NC. Neutrophils use superoxide to control bacterial infection at a distance. Plos Pathogens. 2018;14(7). doi: ARTN e100715710.1371/journal.ppat.1007157. PubMed PMID: WOS:000440351300015.
37. Copenhaver AM, Casson CN, Nguyen HT, Duda MM, Shin S. IL-1R signaling enables bystander cells to overcome bacterial blockade of host protein synthesis. Proc Natl Acad Sci U S A. 2015;112(24):7557-62. Epub 2015/06/03. doi: 10.1073/pnas.1501289112. PubMed PMID: 26034289; PubMed Central PMCID: PMCPMC4475993.
38. Friedman H, Yamamoto Y, Klein TW. *Legionella pneumophila* pathogenesis and immunity. Semin Pediatr Infect Dis. 2002;13(4):273-9. Epub 2002/12/20. doi: 10.1053/spid.2002.127206. PubMed PMID: 12491233.
39. Asrat S, de Jesus DA, Hempstead AD, Ramabhadran V, Isberg RR. Bacterial pathogen manipulation of host membrane trafficking. Annu Rev Cell Dev Biol. 2014;30:79-109. doi: 10.1146/annurev-cellbio-100913-013439. PubMed PMID: 25103867.
40. Archer KA, Alexopoulou L, Flavell RA, Roy CR. Multiple MyD88-dependent responses contribute to pulmonary clearance of *Legionella pneumophila*. Cell Microbiol. 2009;11(1):21-36. Epub 2008/09/11. doi: CMI1234 [pii]10.1111/j.1462-5822.2008.01234.x. PubMed PMID: 18782351.
41. Archer KA, Roy CR. MyD88-dependent responses involving toll-like receptor 2 are important for protection and clearance of *Legionella pneumophila* in a mouse model of Legionnaires' disease. Infect Immun. 2006;74(6):3325-33. Epub 2006/05/23. doi: 74/6/3325 [pii]10.1128/IAI.02049-05. PubMed PMID: 16714560; PubMed Central PMCID: PMC1479235.
42. Hawn TR, Smith KD, Aderem A, Skerrett SJ. Myeloid differentiation primary response gene (88)- and toll-like receptor 2-deficient mice are susceptible to infection with aerosolized *Legionella pneumophila.* J Infect Dis. 2006;193(12):1693-702. Epub 2006/05/17. doi: 10.1086/504525. PubMed PMID: 16703513.
43. Sporri R, Joller N, Albers U, Hilbi H, Oxenius A. MyD88-dependent IFN-gamma production by NK cells is key for control of *Legionella pneumophila* infection. J Immunol. 2006;176(10):6162-71. Epub 2006/05/04. doi: 176/10/6162 [pii]. PubMed PMID: 16670325.
44. Mallama CA, McCoy-Simandle K, Cianciotto NP. The Type II Secretion System of *Legionella pneumophila* Dampens the MyD88 and Toll-Like Receptor 2 Signaling Pathway in Infected Human Macrophages. Infect Immun. 2017;85(4). Epub 2017/02/01. doi: 10.1128/IAI.00897-16. PubMed PMID: 28138020; PubMed Central PMCID: PMCPMC5364298.
45. Hosseini R, Lamers GE, Soltani HM, Meijer AH, Spaink HP, Schaaf MJ. Efferocytosis and extrusion of leukocytes determine the progression of early mycobacterial pathogenesis. J Cell Sci. 2016;129(18):3385-95. Epub 2016/07/30. doi: 10.1242/jcs.135194. PubMed PMID: 27469488.

46. Rosowski EE, Raffa N, Knox BP, Golenberg N, Keller NP, Huttenlocher A. Macrophages inhibit *Aspergillus fumigatus* germination and neutrophil-mediated fungal killing. PLoS Pathog. 2018;14(8):e1007229. Epub 20180802. doi: 10.1371/journal.ppat.1007229. PubMed PMID: 30071103; PubMed Central PMCID: PMCPMC6091969.
47. Saralahti A, Ramet M. Zebrafish and Streptococcal Infections. Scand J Immunol. 2015;82(3):174-83. doi: 10.1111/sji.12320. PubMed PMID: 26095827.
48. Scherer AK, Blair BA, Park J, Seman BG, Kelley JB, Wheeler RT. Redundant Trojan horse and endothelial-circulatory mechanisms for host-mediated spread of *Candida albicans* yeast. PLoS Pathog. 2020;16(8):e1008414. Epub 20200810. doi: 10.1371/journal.ppat.1008414. PubMed PMID: 32776983; PubMed Central PMCID: PMCPMC7447064.
49. Tesh MJ, Miller RD. Amino acid requirements for *Legionella pneumophila* growth. J Clin Microbiol. 1981;13(5):865-9.
50. Fonseca MV, Swanson MS. Nutrient salvaging and metabolism by the intracellular pathogen *Legionella pneumophila*. Frontiers in cellular and infection microbiology. 2014;4:12. doi: 10.3389/fcimb.2014.00012. PubMed PMID: 24575391; PubMed Central PMCID: PMCPMC3920079.
51. Hauslein I, Manske C, Goebel W, Eisenreich W, Hilbi H. Pathway analysis using (13) C-glycerol and other carbon tracers reveals a bipartite metabolism of *Legionella pneumophila*. Mol Microbiol. 2016;100(2):229-46. doi: 10.1111/mmi.13313. PubMed PMID: 26691313.
52. Hauslein I, Sahr T, Escoll P, Klausner N, Eisenreich W, Buchrieser C. *Legionella pneumophila* CsrA regulates a metabolic switch from amino acid to glycerolipid metabolism. Open Biol. 2017;7(11). doi: 10.1098/rsob.170149. PubMed PMID: 29093212.
53. Fraher D, Sanigorski A, Mellett NA, Meikle PJ, Sinclair AJ, Gibert Y. Zebrafish Embryonic Lipidomic Analysis Reveals that the Yolk Cell Is Metabolically Active in Processing Lipid. Cell Rep. 2016;14(6):1317-29. Epub 2016/02/09. doi: 10.1016/j.celrep.2016.01.016. PubMed PMID: 26854233.
54. Hiller M, Lang C, Michel W, Flieger A. Secreted phospholipases of the lung pathogen *Legionella pneumophila*. Int J Med Microbiol. 2017. doi: 10.1016/j.ijmm.2017.10.002. PubMed PMID: 29108710.
55. Brieland J, Freeman P, Kunkel R, Chrisp C, Hurley M, Fantone J, et al. Replicative *Legionella pneumophila* lung infection in intratracheally inoculated A/J mice. A murine model of human Legionnaires' disease. Am J Pathol. 1994;145(6):1537-46. Epub 1994/12/01. PubMed PMID: 7992856; PubMed Central PMCID: PMCPMC1887509.
56. Glavin FL, Winn WC, Jr., Craighead JE. Ultrastructure of lung in Legionnaires' disease. Observations of three biopsies done during the Vermont epidemic. Ann Intern Med. 1979;90(4):555-9. Epub 1979/04/01. doi: 10.7326/0003-4819-90-4-555. PubMed PMID: 434634.
57. Horwitz MA. Formation of a novel phagosome by the Legionnaires' disease bacterium (*Legionella pneumophila*) in human monocytes. J Exp Med. 1983;158(4):1319-31.
58. Horwitz MA, Silverstein SC. Legionnaires' disease bacterium (*Legionella pneumophila*) multiples intracellularly in human monocytes. J Clin Invest. 1980;66(3):441-50. PubMed PMID: 7190579.
59. Jager J, Marwitz S, Tiefenau J, Rasch J, Shevchuk O, Kugler C, et al. Human lung tissue explants reveal novel interactions during *Legionella pneumophila* infections. Infect Immun. 2014;82(1):275-85. Epub 2013/10/30. doi: 10.1128/IAI.00703-13. PubMed PMID: 24166955; PubMed Central PMCID: PMCPMC3911869.
60. Copenhaver AM, Casson CN, Nguyen HT, Fung TC, Duda MM, Roy CR, et al. Alveolar macrophages and neutrophils are the primary reservoirs for *Legionella pneumophila* and mediate cytosolic surveillance of type IV secretion. Infect Immun. 2014;82(10):4325-36. Epub 2014/08/06. doi: 10.1128/IAI.01891-14. PubMed PMID: 25092908; PubMed Central PMCID: PMCPMC4187856.
61. Bennett CM, Kanki JP, Rhodes J, Liu TX, Paw BH, Kieran MW, et al. Myelopoiesis in the zebrafish, *Danio rerio*. Blood. 2001;98(3):643-51. Epub 2001/07/27. doi: 10.1182/blood.v98.3.643. PubMed PMID: 11468162.

954 62. Le Guyader D, Redd MJ, Colucci-Guyon E, Murayama E, Kissa K, Briolat V, et al. Origins and
955 unconventional behavior of neutrophils in developing zebrafish. Blood. 2008;111(1):132-41. Epub
956 2007/09/19. doi: 10.1182/blood-2007-06-095398. PubMed PMID: 17875807.
957 63. Willett CE, Cortes A, Zuasti A, Zapata AG. Early hematopoiesis and developing lymphoid organs in
958 the zebrafish. Dev Dyn. 1999;214(4):323-36. Epub 1999/04/23. doi: 10.1002/(SICI)1097-
959 0177(199904)214:4<323::AID-AJA5>3.0.CO;2-3. PubMed PMID: 10213388.
960 64. Mesureur J, Feliciano JR, Wagner N, Gomes MC, Zhang L, Blanco-Gonzalez M, et al. Macrophages,
961 but not neutrophils, are critical for proliferation of *Burkholderia cenocepacia* and ensuing host-
962 damaging inflammation. PLoS Pathog. 2017;13(6):e1006437. Epub 2017/06/27. doi:
963 10.1371/journal.ppat.1006437. PubMed PMID: 28651010; PubMed Central PMCID:
964 PMCPMC5501683.
965 65. Prajsnar TK, Cunliffe VT, Foster SJ, Renshaw SA. A novel vertebrate model of *Staphylococcus*
966 *aureus* infection reveals phagocyte-dependent resistance of zebrafish to non-host specialized
967 pathogens. Cell Microbiol. 2008;10(11):2312-25. Epub 2008/08/22. doi: 10.1111/j.1462-
968 5822.2008.01213.x. PubMed PMID: 18715285.
969 66. Jault C, Pichon L, Chluba J. Toll-like receptor gene family and TIR-domain adapters in *Danio rerio*.
970 Mol Immunol. 2004;40(11):759-71. Epub 2003/12/23. doi: 10.1016/j.molimm.2003.10.001.
971 PubMed PMID: 14687933.
972 67. Meijer AH, Gabby Krens SF, Medina Rodriguez IA, He S, Bitter W, Ewa Snaar-Jagalska B, et al.
973 Expression analysis of the Toll-like receptor and TIR domain adaptor families of zebrafish. Mol
974 Immunol. 2004;40(11):773-83. Epub 2003/12/23. doi: 10.1016/j.molimm.2003.10.003. PubMed
975 PMID: 14687934.
976 68. Akira S, Takeda K. Toll-like receptor signalling. Nat Rev Immunol. 2004;4(7):499-511. Epub
977 2004/07/02. doi: 10.1038/nri1391. PubMed PMID: 15229469.
978 69. Wik JA, Phung D, Kolan S, Haraldsen G, Skalhegg BS, Hol Fosse J. Inflammatory activation of
979 endothelial cells increases glycolysis and oxygen consumption despite inhibiting cell proliferation.
980 FEBS Open Bio. 2021;11(6):1719-30. Epub 2021/05/13. doi: 10.1002/2211-5463.13174. PubMed
981 PMID: 33979025; PubMed Central PMCID: PMCPMC8167874.
982 70. Hall C, Flores MV, Storm T, Crosier K, Crosier P. The zebrafish lysozyme C promoter drives myeloid-
983 specific expression in transgenic fish. Bmc Dev Biol. 2007;7. doi: Artn 4210.1186/1471-213x-7-42.
984 PubMed PMID: WOS:000246708100001.
985 71. Renshaw SA, Loynes CA, Trushell DM, Elworthy S, Ingham PW, Whyte MK. A transgenic zebrafish
986 model of neutrophilic inflammation. Blood. 2006;108(13):3976-8. Epub 2006/08/24. doi:
987 10.1182/blood-2006-05-024075. PubMed PMID: 16926288.
988 72. van Leeuwen LM, Evans RJ, Jim KK, Verboom T, Fang X, Bojarczuk A, et al. A transgenic zebrafish
989 model for the *in vivo* study of the blood and choroid plexus brain barriers using claudin 5. Biol
990 Open. 2018;7(2). Epub 2018/02/14. doi: 10.1242/bio.030494. PubMed PMID: 29437557; PubMed
991 Central PMCID: PMCPMC5861362.
992 73. van der Vaart M, van Soest JJ, Spaink HP, Meijer AH. Functional analysis of a zebrafish myd88
993 mutant identifies key transcriptional components of the innate immune system. Dis Model Mech.
994 2013;6(3):841-54. doi: 10.1242/dmm.010843. PubMed PMID: WOS:000318847400030.
995 74. Tiaden A, Spirig T, Weber SS, Bruggemann H, Bosshard R, Buchrieser C, et al. The *Legionella*
996 *pneumophila* response regulator LqsR promotes host cell interactions as an element of the
997 virulence regulatory network controlled by RpoS and LetA. Cell Microbiol. 2007;9(12):2903-20.
998 Epub 2007/07/07. doi: CMI1005 [pii]10.1111/j.1462-5822.2007.01005.x. PubMed PMID:
999 17614967.
1000 75. Levraud JP, Colucci-Guyon E, Redd MJ, Lutfalla G, Herbomel P. In vivo analysis of zebrafish innate
1001 immunity. Methods Mol Biol. 2008;415:337-63. doi: 10.1007/978-1-59745-570-1_20. PubMed
1002 PMID: 18370164.
1003 76. Brannon MK, Davis JM, Mathias JR, Hall CJ, Emerson JC, Crosier PS, et al. *Pseudomonas aeruginosa*
1004 Type III secretion system interacts with phagocytes to modulate systemic infection of zebrafish

1005 embryos. Cell Microbiol. 2009;11(5):755-68. Epub 2009/02/12. doi: 10.1111/j.1462-
1006 5822.2009.01288.x. PubMed PMID: 19207728; PubMed Central PMCID: PMCPMC2933946.
1007 77. Colucci-Guyon E, Rifflet A, Saint-Auret S, da Costa A, Boucontet L, Laval T, et al. Spatiotemporal
1008 analysis of mycolactone distribution i*n vivo* reveals partial diffusion in the central nervous system.
1009 PLoS Negl Trop Dis. 2020;14(12):e0008878. Epub 2020/12/03. doi:
1010 10.1371/journal.pntd.0008878. PubMed PMID: 33264290; PubMed Central PMCID:
1011 PMCPMC7710047.
1012

1013 **FIGURES LEGENDS**

1014

1015 **Figure 1. Zebrafish larvae are susceptible to intravenous *L. pneumophila* infection in a dose**
1016 **dependent manner**. **A)** Scheme of the experimental set up of bacterial infection using zebrafish. A
1017 72hpf zebrafish larva is shown. Bacteria are injected in the bloodstream (iv) via the caudal vein
1018 (green arrow). **B)** Survival curves (three independent experiments pooled) of zebrafish larvae
1019 injected with WT-GFP Low Dose (WT LD) (blue curve, n=60) or High Dose (HD) (red curve, n=60), or
1020 with Δ*dotA*-GFP Low Dose (Δ*dotA* LD) (green curve, n=12) or High Dose (Δ*dotA* HD) (green curve,
1021 n=36), and incubated at 28°C. Control non-injected fish (CTRL, black curve; n= 72). $P < 0.05$ was
1022 considered statistically significant (symbols: **** $P < 0.0001$; ***$P < 0.001$; **$P < 0.01$; *$P < 0.05$. **C**)
1023 Bacterial burden evaluation by quantification of % of fluorescent pixel counts from images of
1024 individual injected larvae followed overtime from 0 to 72hpi. Each larva was imaged daily, and
1025 images were analysed with Fiji for bacterial burden quantification. Five experiments have been
1026 pooled, for a total of 28 larvae for WT LD and LD, 18 for Δ*dotA* HD. $P < 0.05$ was considered
1027 statistically significant (symbols: **** $P < 0.0001$; ***$P < 0.001$; **$P < 0.01$; *$P < 0.05$. No symbol on
1028 graphs means that not statistically differences were observed. -**D)** Representative images of
1029 *L. pneumophila* dissemination, determined by live imaging using a fluorescence stereomicroscope, of
1030 zebrafish AB larvae infected with a LD or a HD of WT-GFP, or a HD of Δ*dotA*-GFP. Individual infected
1031 larvae were followed over time by live imaging at 4h, 24h, 48h, and 72h post injection. GFP
1032 fluorescence of the injected bacteria is shown. **E)** Quantification of bacterial dissemination overtime.
1033 Larvae injected with LD, HD LD or Δ*dotA* HD were imaged overtime, and then scored for the GFP +
1034 bacteria absolute presence for each larva overtime. Larvae were scored as "infected" when they
1035 showed at least one small detectable GFP+ dot. Data obtained were plotted as % of larvae with
1036 bacteria in the body (tail, trunk, head; blue curve), or in the yolk (pink curve). 11 independent
1037 experiments have been plotted (representing a total of n=69 WT LD; n=58 WT HD; n=54 Δ*dotA* HD
1038 infected larvae). **F**) Scheme of a 72hpi larva with body (light blue) and yolk (pink) region highlighted.
1039 Green dot in the yolk represents bacteria burden.

1040

1041 **Figure 2. Bloodstream *L. pneumophila* establish a proliferative niche in the yolk causing a**
1042 **persistent local infection**. **A)** Survival curves (two independent experiments pooled) of zebrafish
1043 larvae injected with WT-GFP Low Dose (WT LD) (blue curve, n=48) or High Dose (HD) (red curve,
1044 n=48), or with Δ*dotA*-GFP Low Dose (Δ*dotA* LD) (magenta curve, n=48) or High Dose (Δ*dotA* HD)
1045 (green curve, n=48), and incubated at 28°C. Non-injected fish (CTRL, black curve; n= 48). **B)** Bacterial
1046 burden evaluation by quantification of % of fluorescent pixel counts on individual injected larvae
1047 followed overtime by 0 to 48hpi. Each larva was imaged daily, and images were analysed with Fiji for

1048 bacterial burden evaluation. One experiment plotted, 6 larvae per condition. P < 0.05 was considered
1049 statistically significant (symbols: **** P < 0.0001; ***P < 0.001; **P < 0.01; *P < 0.05. No symbol on
1050 graphs means that not statistically differences were observed. **C)** Representative images of
1051 *L. pneumophila* localization, determined by live imaging using a fluorescence stereomicroscope, of
1052 zebrafish larvae infected with a LD or a HD of WT-GFP, or a LD or a HD of Δ*dotA*-GFP. Individual
1053 infected larvae were followed over time by live imaging at 4h, 24h, 48h, and 72hpi. GFP fluorescence
1054 of the injected bacteria is shown. Dotted circle highlights GFP bacteria in the yolk. **D)** Representative
1055 maximum intensity projection of confocal acquisition of a 72hpi zebrafish larva injected in the
1056 bloodstream with HD of WT-GFP, mounted laterally and live imaged using high resolution confocal
1057 fluorescence microscope, showing bacteria growing in the yolk and yolk tube region. The x-y-z raw
1058 data were post treated with the LEICA lighting application for reducing noise and processed with
1059 Imaris for 3D volume rendering. Related to Movie S1. **E)** Imaris 3D reconstruction and volume
1060 rendering of the *L. pneumophila* growth (GFP labelling) in the yolk of *kdrl:*ras-mCherry (red vessels)
1061 infected larva at 72hpi, showed laterally. Overlay of GFP and mCherry is shown; BF is shown to help
1062 to visualize the yolk region and host anatomy. Related to Movie S2. Scale bar = 50mm.
1063
1064 **Figure 3. Characterization of the *L. pneumophila* foci growing in the yolk region of zebrafish larvae.**
1065 **A)** Scheme of 72hpf with body (light blue) and yolk region (pink) highlighted; the yolk sustaining
1066 *L. pneumophila* growing has been indicated with green dots**. B**) Imaris 3D reconstruction and volume
1067 rendering of the *L. pneumophila* growth in the yolk of 72hpi *mfap4*: mCherry larva (red
1068 macrophages) injected in the bloodstream with HD of WT-GFP at 72hpf, shown laterally. Inset shows
1069 the maximum intensity projection of the *L. pneumophila* foci of the same larva mounted ventrally.
1070 Scale bar = 20mm. Related to Movie S3. **C)** Imaris 3D reconstruction and volume rendering of the
1071 *L. pneumophila* growth in the yolk of *lyz*:DsRed (red neutrophils) infected larva at 72hpi, showed
1072 laterally. Scale bar = 20mm. Related to Movie S4. **D)** Quantification of bacterial burden in the yolk
1073 overtime. Larvae injected with LD, HD WT, or Δ*dotA* HD were imaged overtime, and then scored for
1074 the GFP + bacteria absolute presence in the yolk for each larva overtime. Larvae were scored as
1075 "infected" when they showed at least one small detectable GFP+ dot. Data obtained were plotted as
1076 % of larvae with bacteria in the in the yolk upon LD (blue curve), HD (red curve) WT or Δ*dotA* HD
1077 (green curve) injection overtime. 11 independent experiments have been plotted (representing a
1078 total of n=69 WT LD; n=58 WT HD; n=54 Δ*dotA* HD infected larvae) **E)** Time frame extracted from a
1079 4D acquisition of *L. pneumophila* growth in the yolk between 48 and 72hpi of *mfap4*: mCherry larva
1080 (red macrophages) injected in the bloodstream with HD of WT-GFP shown laterally. Imaris 4D
1081 reconstruction and volume rendering of the bacteria aggregate and interaction with macrophages.
1082 The yolk has been manually highlighted (in blue) with Imaris. Scale bar: 10. Related to Movie S5. **F)**

1083 Quantification of bacterial burden in the whole body, in the body or in the yolk region versus
1084 macrophage or neutrophil quantification in the body or in the yolk region in HD WT-GFP infected
1085 larvae followed overtime. Two independent experiments plotted for each phagocyte type (total of 11
1086 larvae for macrophage and 11 larvae for neutrophil quantification). Quantification of the
1087 fluorescence images (GFP bacteria and RFP leukocytes) was done using CellProfiler software. $P < 0.05$
1088 was considered statistically significant (symbols: **** $P < 0.0001$; ***$P < 0.001$; **$P < 0.01$; *$P <$
1089 0.05). No symbol on graphs means that not statistically differences were observed.
1090
1091 **Figure 4. *L. pneumophila* high dose injection results in (systemic) macrophage and neutrophil**
1092 **death. A)** Macrophage counts of control larvae (black symbols) or upon Low Dose (blue symbols) or
1093 High Dose of WT-GFP (red symbols), or High Dose (green symbols) of Δ*dotA* -GFP injection.
1094 Macrophages were counted manually from images taken on live infected larvae over time from T0 to
1095 T72hpi, using ImageJ software, and results were plotted using GraphPad Prism® software.
1096 Mean±SEM are also shown (horizontal bars). Data plotted are from two pooled independent
1097 experiments (n=12 larvae scored for each condition). $P < 0.05$ was considered statistically significant
1098 (symbols: **** $P < 0.0001$; ***$P < 0.001$; **$P < 0.01$; *$P < 0.05$). No symbol on graphs means that not
1099 statistically differences were observed. **B)** Frames extracted from maximum intensity projection of *in*
1100 *vivo* time-lapse confocal fluorescence microscopy of 72hpf Tg*(mfap4::mCherryF*) larvae injected in
1101 the bloodstream (iv) with a LD, HD (of WT-GFP or a HD of Δ*dotA*-GFP (upper panel) or
1102 Tg(*LysC::DsRed)*^{nz50} in the bloodstream with a LD, HD of WT-GFP or a HD of Δ*dotA*-GFP (lower panel)
1103 to follow macrophage bacteria interaction overtime during the first 16hpi. Overlay of green (*L.*
1104 *pneumophila*) and red (leucocytes) fluorescence of the caudal area of the larvae (region boxed in the
1105 scheme on the right of the panel) is shown. BF helps for anatomical region indication. Representative
1106 of n= 12 to 16 injected larvae for each condition. Scale bar: 50μm. See also related Movies S6. **C)**
1107 macrophage *L pneumophila* interaction at 72hpi captured at high resolution upon HD WT injection.
1108 Live bacteria are inside zebrafish macrophages suggesting the establishment of a replicative niche, as
1109 documented for cultured mammalian macrophages or amoebae. Representative of n= 15 scored
1110 infected larvae. Overlay of green (GFP bacteria), red (mCherry macrophages) and BF is shown. Scale
1111 bar= 10mm
1112
1113 **Figure 5. *L. pneumophila* interaction with neutrophils and neutrophil counts upon bloodstream**
1114 **injection of LD, HD WT GFP or HD ΔdotA *L pneumophila*.**
1115 **A)** Neutrophil counts from control larvae (CTRL, black symbols) or Low Dose or High Dose of WT-GFP
1116 (blue or red symbols), or High Dose of Δ*dotA*-GFP (green symbols) injected larvae. Data plotted in the
1117 same way as for macrophage counts in Fig 4. Two pooled independent experiments (n=10 larvae

1118 scored for each condition). P < 0.05 was considered statistically significant (symbols: **** P < 0.0001;
1119 ***P < 0.001; **P < 0.01; *P < 0.05). No symbol on graphs means that not statistically differences
1120 were observed. **B)** Frames extracted from maximum intensity projection of *in vivo* time-lapse
1121 confocal fluorescence microscopy of 72hpf Tg(*LysC::DsRed)*^{nz50} in the bloodstream (iv) with a LD, HD
1122 of WT-GFP or a HD of Δ*dotA*-GFP (lower panel) to follow neutrophil interaction with *L. pneumophila*
1123 immediately upon injection for 16hpi. Images were taken from time lapse at different time points
1124 (0hpi, 2hpi, 4hpi, 8hpi and 16hpi). Overlay of green (*L. pneumophila*) and red (neutrophils)
1125 fluorescence of the caudal area of the larvae (region boxed in the scheme on the right of the panel) is
1126 shown. Data representative of n= 12 to 16 larvae scored. Scale bar: 50μm. See also related Movies
1127 S7. **C)** Details of a dying phagocytosing neutrophil, progressively rounding-up and loosing
1128 fluorescence upon HD WT injection. Arrowheads point to the dying phagocytosing neutrophils.
1129 Representatives of n= 14 larvae scored. Scale bar=10mm. See also related Movie S8.
1130
1131 **Figure 6. Macrophages are crucial to restrict *Legionella pneumophila* dissemination**
1132 **A)** Survival curves of CTRL morphant zebrafish larvae injected with a Low Dose (LD) (blue dashed
1133 curve, n=34 larvae) or a High Dose (HD) (red dashed curve, n=34) of WT-GFP, or with a HD (green
1134 dashed curve, n=24) of Δ*dotA* -GFP, and *spi1b* morphant zebrafish larvae injected with a LD (blue
1135 curve, n=48) or a HD (red curve, n=48) of WT-GFP, or with a High Dose (HD) (green curve, n=48) of
1136 Δ*dotA* -GFP. Non-injected CTRL morphant fish (black dashed curve, n=48), and *spi1b* morphant fish
1137 (black curves, n=48) were used as control. Infected and control larvae were incubated at 28°C. Data
1138 plotted are from two pooled independent experiments. **B)** and **E**) Bacterial burden evaluation by
1139 quantification of % of fluorescent pixel counts on individual injected larvae followed overtime by 0 to
1140 72hpi. Each larva was imaged daily, and images were analysed with Fiji for bacterial burden
1141 evaluation. One experiment per phagocyte type plotted, 6 larvae for each condition. **D)** Survival
1142 curves of CTRL morphant zebrafish larvae injected with a LD (blue dashed curve, n=36) or a HD (red
1143 dashed curve, n=36) of WT-GFP, or with a HD (green dashed curve, n=24) of Δ*dotA* -GFP, and *csf3r*
1144 morphant zebrafish larvae injected with a LD (blue curve, n=24) or a HD (red curve, n=36) of WT-GFP,
1145 or with a HD (green curve, n=36) of Δ*dotA* -GFP. Non-injected CTRL morphant fish (black dashed
1146 curve, n=48), and *csf3r* morphant fish (black curve, n=36) were used as control. Data plotted are from
1147 two pooled independent experiments. Significant differences are highlighted with stars (see
1148 experimental procedure for statistical analysis) **C)** and **F)** Representative images of *L. pneumophila*
1149 dissemination, determined by live imaging using a fluorescence stereomicroscope, of
1150 Tg*(mfap4::mCherryF*) *spi1b* morphant larvae (**C**) and of Tg(*LysC::DsRed)*^{nz50} (**F)** *csf3r* morphant larvae
1151 non infected, or infected with a LD or a HD of WT-GFP, or a HD of Δ*dotA*-GFP. The same infected
1152 larvae were live imaged 4h, 24h, 48h, and 72h post *L. pneumophila* injection. Overlay of GFP and

1153 mCherry fluorescence is shown. P < 0.05 was considered statistically significant (symbols: **** P <
1154 0.0001; ***P < 0.001; **P < 0.01; *P < 0.05). No symbol on graphs means that not statistically
1155 differences were observed.
1156
1157 **Figure 7. Cytokine gene induction upon *L. pneumophila* infection and Zebrafish larva Immunity to**
1158 ***L. pneumophila* is independent from signalling through MyD88 or compensated by other signalling**
1159 **pathways**. **A-D)** Cytokine gene (*il1b*, *tnfa, ifng1, ifng2*) induction was measured from non-injected
1160 larvae as control (CTRL, dashed black curves) and individual zebrafish larvae injected with a LD (blue
1161 curves) or a HD (red curves) of WT-GFP, or a HD of Δ*dotA*-GFP (green curves). Data plotted are from 2
1162 pooled experiments (n=10 larvae for each condition) for *il1b* and *tnfa,* and from 1 experiment (n=5
1163 larvae for each condition) for *ifng1* and *ifng2*; individual values are shown, and curves correspond to
1164 the medians. Statistical analyses are shown in the table under each graph. **E)** Survival curves of CTRL
1165 zebrafish larvae injected with WT-GFP Low Dose (LD) (blue dashed curve) or High Dose (HD) (red
1166 dashed curve), or with Δ*dotA* -GFP HD (green dashed curve), and *myd88*^{hu3568} mutant zebrafish larvae
1167 injected with WT-GFP LD (blue curve) or HD (red curve), or with Δ*dotA* -GFP HD (green curve). Non-
1168 injected CTRL larvae (black dashed curves), and *myd88*^{hu3568} mutant larvae (black curves) were used
1169 as control. Infected and control larvae (n= 72 fish for *myd88*^{hu3568} mutant conditions and n= 57 fish
1170 for CTRL conditions) were incubated at 28°C. Data plotted are from 3 pooled independent
1171 experiments. **F)** Bacterial burden evaluation by quantification of % of fluorescent pixel counts on
1172 individual injected larvae followed overtime from 0 to 72hpi. Each larva was imaged daily, and
1173 images were analysed with Fiji for bacterial burden evaluation. Two pooled experiments, 8 larvae for
1174 each condition. P < 0.05 was considered statistically significant (symbols: **** P < 0.0001; ***P <
1175 0.001; **P < 0.01; *P < 0.05). No symbol on graphs means that not statistically differences were
1176 observed.
1177

1178 Figure 1

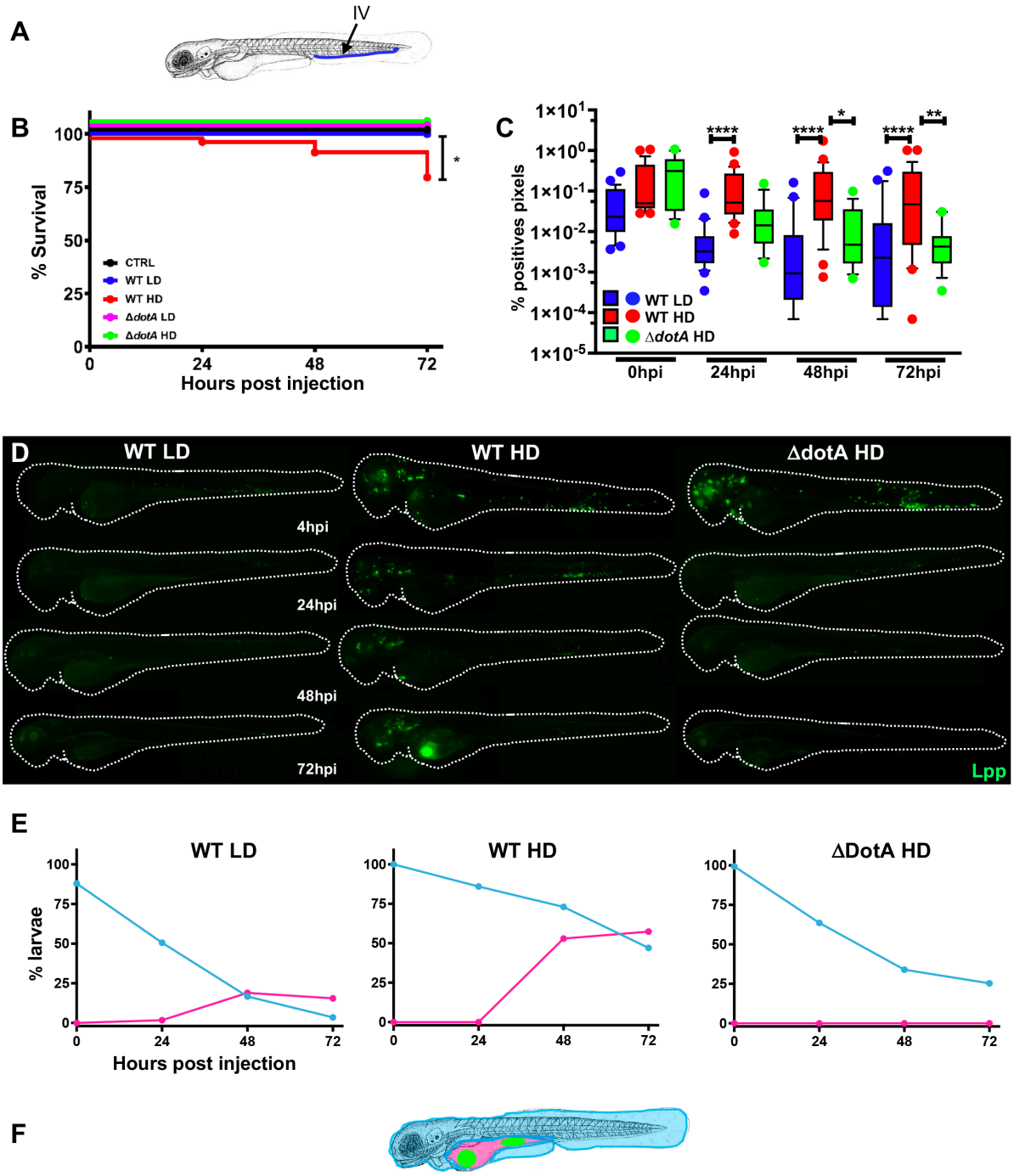

1179

1180

1181 Figure 2

1182

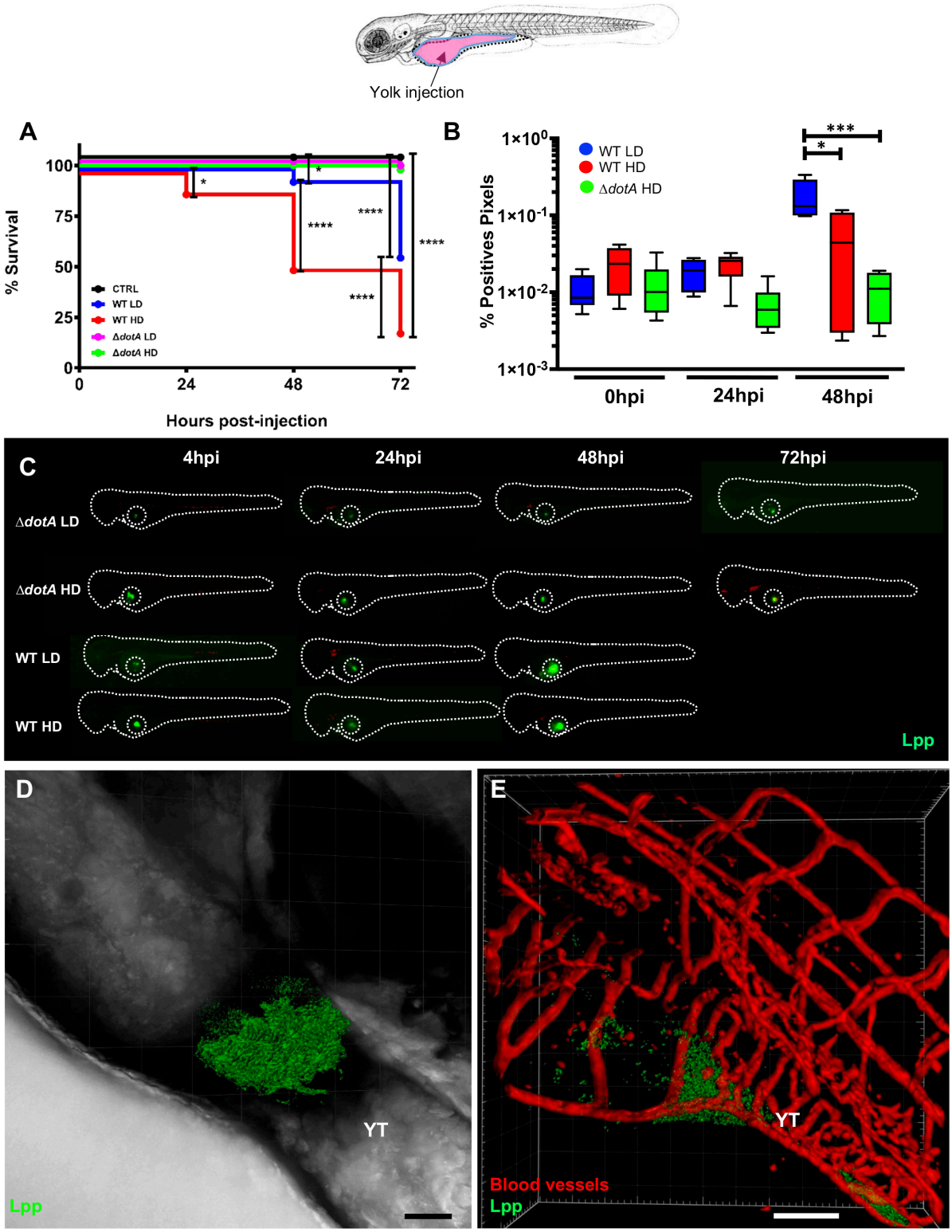

1183

1184 Figure 3

1185

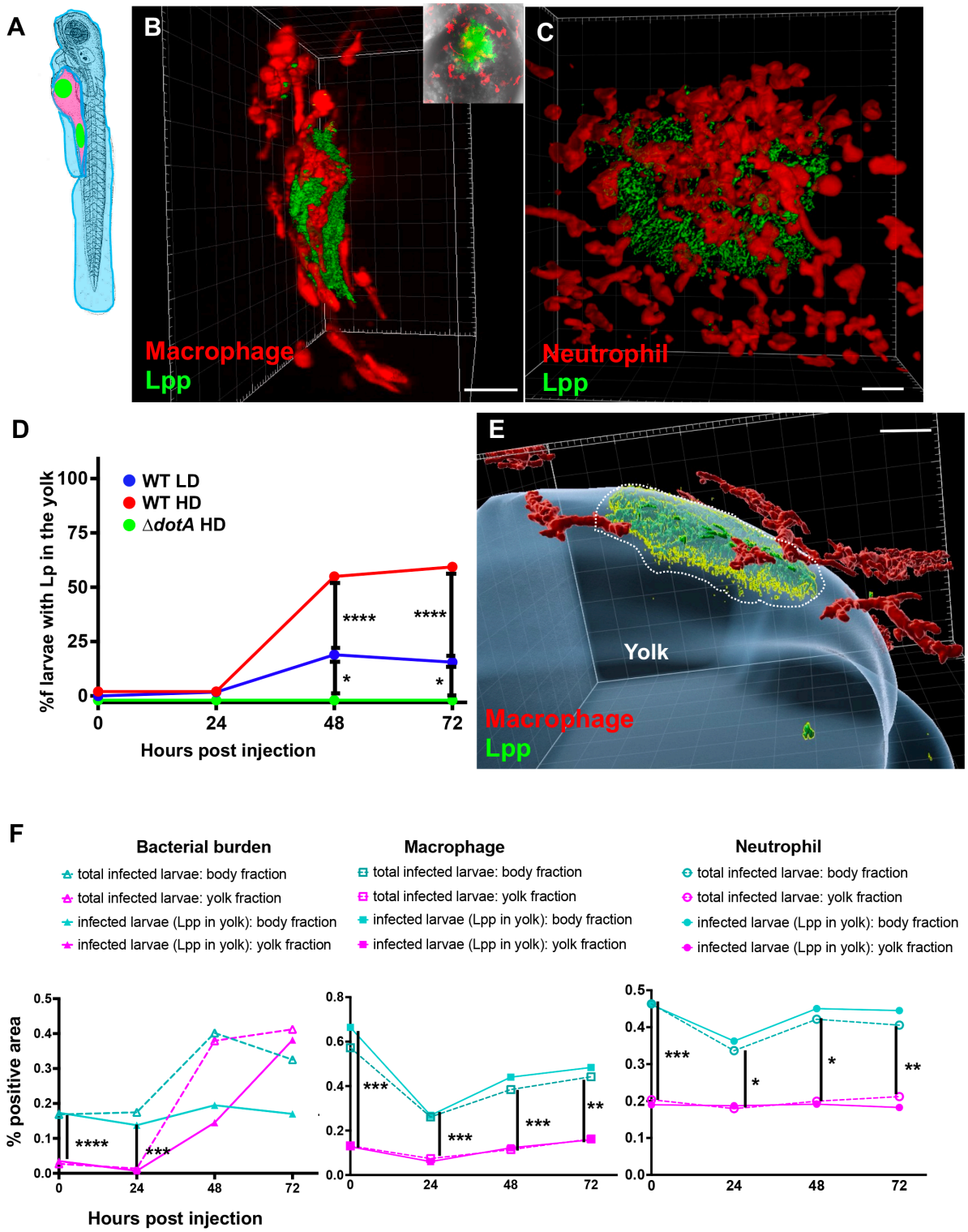

1186

1187 Figure 4

1188

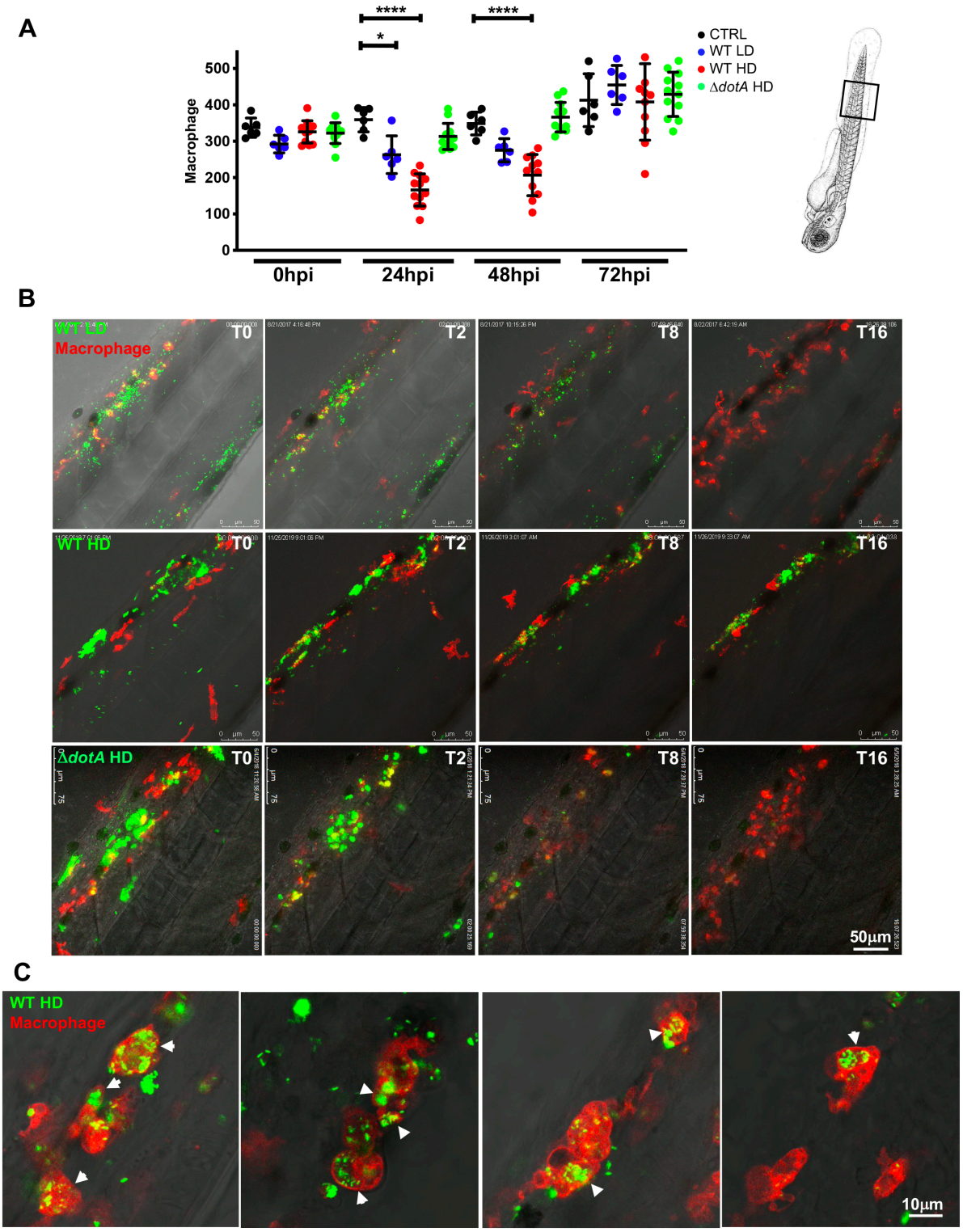

1189

1190

1191 Figure 5

1192

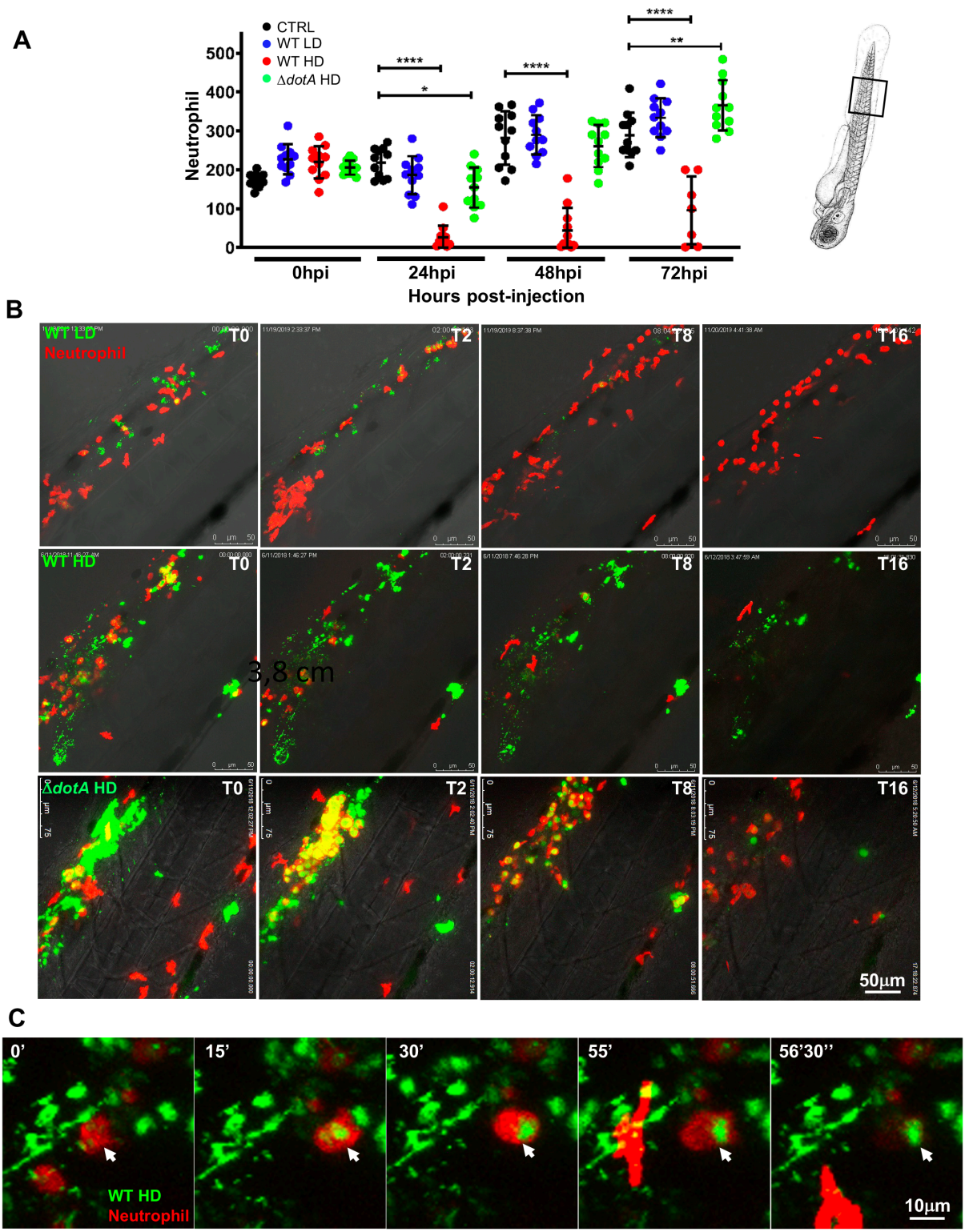

1193

1194

Figure 6

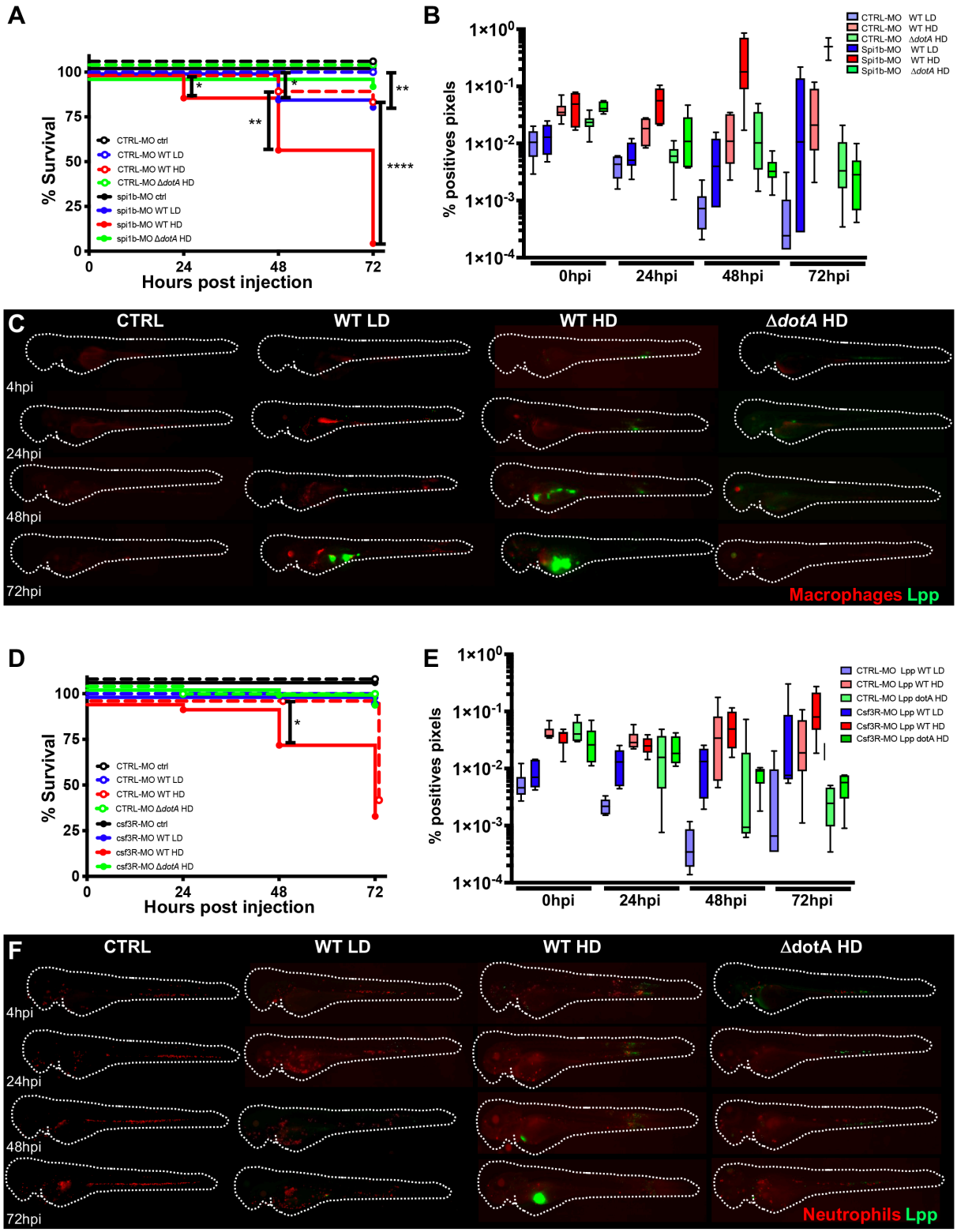
A
% Survival
Hours post injection
CTRL-MO ctrl
CTRL-MO WT LD
CTRL-MO WT HD
CTRL-MO ΔdotA HD
spi1b-MO ctrl
spi1b-MO WT LD
spi1b-MO WT HD
spi1b-MO ΔdotA HD
B
% positives pixels
0hpi
24hpi
48hpi
72hpi
CTRL-MO WT LD
CTRL-MO WT HD
CTRL-MO ΔdotA HD
Spi1b-MO WT LD
Spi1b-MO WT HD
Spi1b-MO ΔdotA HD
C
CTRL
WT LD
WT HD
ΔdotA HD
4hpi
24hpi
48hpi
72hpi
Macrophages Lpp
D
% Survival
Hours post injection
CTRL-MO ctrl
CTRL-MO WT LD
CTRL-MO WT HD
CTRL-MO ΔdotA HD
csf3R-MO ctrl
csf3R-MO WT LD
csf3R-MO WT HD
csf3R-MO ΔdotA HD
E
% positives pixels
0hpi
24hpi
48hpi
72hpi
CTRL-MO Lpp WT LD
CTRL-MO Lpp WT HD
CTRL-MO Lpp dotA HD
Csf3R-MO Lpp WT LD
Csf3R-MO Lpp WT HD
Csf3R-MO Lpp dotA HD
F
CTRL
WT LD
WT HD
ΔdotA HD
4hpi
24hpi
48hpi
72hpi
Neutrophils Lpp

1198 Figure 7

1199

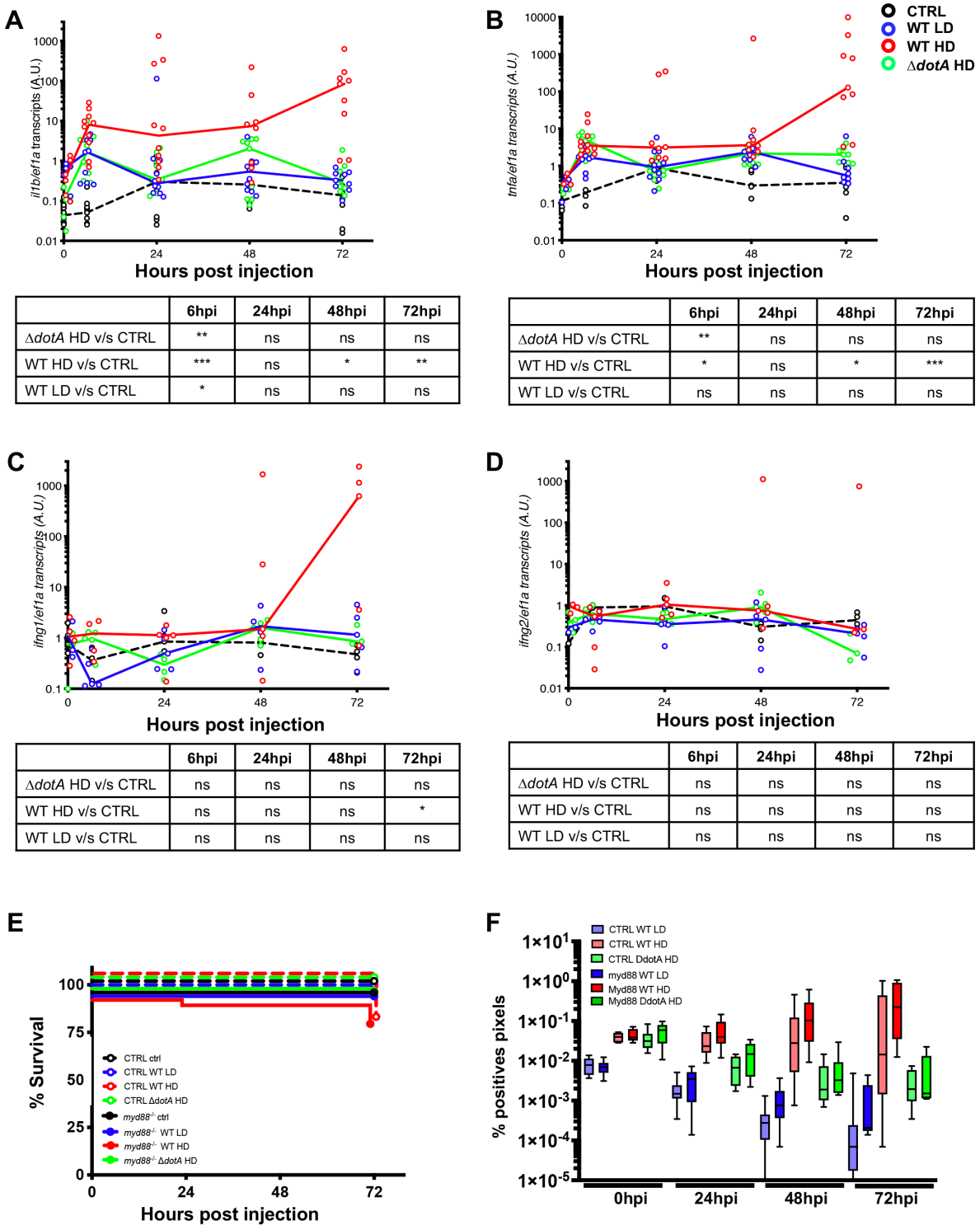

	6hpi	24hpi	48hpi	72hpi
Δ*dotA* HD v/s CTRL	**	ns	ns	ns
WT HD v/s CTRL	***	ns	*	**
WT LD v/s CTRL	*	ns	ns	ns

	6hpi	24hpi	48hpi	72hpi
Δ*dotA* HD v/s CTRL	**	ns	ns	ns
WT HD v/s CTRL	*	ns	*	***
WT LD v/s CTRL	ns	ns	ns	ns

	6hpi	24hpi	48hpi	72hpi
Δ*dotA* HD v/s CTRL	ns	ns	ns	ns
WT HD v/s CTRL	ns	ns	ns	*
WT LD v/s CTRL	ns	ns	ns	ns

	6hpi	24hpi	48hpi	72hpi
Δ*dotA* HD v/s CTRL	ns	ns	ns	ns
WT HD v/s CTRL	ns	ns	ns	ns
WT LD v/s CTRL	ns	ns	ns	ns

1200

1201 $